NACA

RESEARCH MEMORANDUM

AERODYNAMIC CHARACTERISTICS OF BODIES

AT SUPERSONIC SPEEDS

A COLLECTION OF THREE PAPERS

By Alvin Seiff
Ames Aeronautical Laboratory
Carl A. Sandahl
Langley Aeronautical Laboratory
Dean R. Chapman
Ames Aeronautical Laboratory
E. W. Perkins
Ames Aeronautical Laboratory
and F. E. Gowen
Ames Aeronautical Laboratory

NATIONAL ADVISORY COMMITTEE
FOR AERONAUTICS
WASHINGTON

November 9, 1951

AERODYNAMIC CHARACTERISTICS OF BODIES

AT SUPERSONIC SPEEDS

A COLLECTION OF THREE PAPERS

By Alvin Seiff
Ames Aeronautical Laboratory
Carl A. Sandahl
Langley Aeronautical Laboratory
Dean R. Chapman
Ames Aeronautical Laboratory
E. W. Perkins
Ames Aeronautical Laboratory
and F. E. Gowen
Ames Aeronautical Laboratory

THE EFFECT OF NOSE SHAPE ON THE DRAG OF BODIES OF

REVOLUTION AT ZERO ANGLE OF ATTACK[1]

By Alvin Seiff
Ames Aeronautical Laboratory

and Carl A. Sandahl
Langley Aeronautical Laboratory

The subject of this paper is the drag of the nose section of bodies
of revolution at zero angle of attack. The magnitude of the nose drag
in relation to the total drag is very distinctly a function of the body
design and the Mach number. It can range from a very small fraction of
the total drag of the order of 10 percent to a very large fraction as
high as 80 percent. The natural objective of nose design is to minimize
the drag, but this objective is not always the primary one. Sometimes
other factors overshadow the desire for minimum drag. The most con-
spicuous example of this is the proposal of guidance engineers that large-
diameter spheres and other very blunt shapes be used at the nose tip.
This paper will attempt to discuss both phases of the problem, noses for
minimum drag and noses with very blunt tips. The state of the theory will
also be reviewed and recent theoretical developments described, since the
theory still remains a very valuable tool for assaying the effects of com-
promises in design and departure from shapes for which experimental data
are available.

The three best-known theories for computing pressure distributions
and pressure drag for pointed shapes are the Taylor and Maccoll theory
for cones and the method of characteristics and linearized theory for
other shapes. The first two of these methods are the exact inviscid
theories and both have been experimentally verified over a wide range of
conditions. Both are limited, however, the first to a single class of
bodies and the second by the large amount of painstaking labor required
to obtain a single solution. The linearized theory suffers from neither
of these limitations but is restricted to slender shapes at low supersonic
Mach numbers because of assumptions in its development. Therefore, none
of the three best-known methods can be considered a satisfactory design
tool for the full range of Mach numbers and fineness ratios now being
proposed. Two more recent theories represent an improvement in that,
used to supplement each other, they allow more complete coverage of the
working range of Mach numbers and fineness ratios than is provided by
linearized theory and require far less effort to apply than the method of
characteristics. They are the second-order theory of Van Dyke (reference 1)
and the shock-expansion theory of Eggers and Savin (reference 2). The
second-order theory extends the range of accurate application of the line-
arized theory essentially up to its fundamental limit, the Mach number at

[1]This is substantially a reprint of the paper by the same authors which
was presented at the NACA Conference on Aerodynamic Design Problems of Super-
sonic Guided Missiles at the Ames Aeronautical Laboratory on Oct. 2-3, 1951.

which the tip Mach cone is tangent to the nose vertex. Fortunately, the shock-expansion theory is most accurate where second-order theory does not apply. Examples of the application of each of these theories will be shown. Then, a summary chart showing their ranges of application will be presented.

The left-hand part of figure 1 shows an application of second-order theory to a tangent ogive with a nose fineness ratio $(l/d)_n$ of 3.5 at a Mach number M of 3.2. Pressure coefficient is plotted as a function of axial station. The second-order solution is compared with experimental data and a characteristics solution as standards of accuracy and with a linearized solution to show the improvement. The experimental data and the characteristics solution agree almost identically. The second-order solution is about 8 percent high at the tip but coincides with the char-acteristics solution beyond the 50-percent station. The linearized solu-tion is too low at the tip by 45 percent and crosses the experimental curve at the 50-percent station so that its drag error is reduced by com-pensation. In the right-hand part of this figure, shock-expansion theory is applied to a slightly thicker ogive at a higher Mach number, 4.5. Again, the experiment and the characteristics solution disagree only a little. The shock-expansion solution follows the characteristics solu-tion perfectly at first and falls below a little at the rear of the nose.

From this figure it is evident that, under some circumstances at least, these two theories are useful tools for design work. It is desir-able to define, as specifically as possible, the range of conditions over which each can be applied. Experience shows that the accuracy of approxi-mate theories depends on three things, the Mach number, the fineness ratio, and the shape. Recently it has been found that, for a given shape, the ranges of application of the various theories can be stated reasonably well in terms of a single variable, the hypersonic-similarity parameter, which is the ratio of Mach number to fineness ratio. This parameter, hereinafter designated by the symbol K, identifies those conditions for which flow fields will be similar. Increasing the similarity param-eter corresponds to increasing the Mach number at a given fineness ratio, or decreasing the fineness ratio at a given Mach number. In terms of this parameter, the range of application of three theories - linearized, second-order, and shock-expansion - to two shapes, cones and ogives, is presented in figure 2. The drag error of each theory in percent is plotted as a function of K. These curves were obtained by integrating a large number of theoretical pressure distributions of the type shown in the preceding figure to obtain the drag and comparing with exact solu-tions to determine the error. The results show the second-order theory to be accurate within 2 percent for the drag of ogives out very nearly to the fundamental limit of the theory. The second-order theory is even better for cones than for ogives, having a wider range of application and smaller errors at a given value of K. For ogives, it underestimates the drag by 5 percent or less for values of K above 1.2. In contrast, the linearized theory shows errors of 10 to 47 percent for cones and 4 to 17 percent for ogives and is accurate only at values of K of the order of 0.4 or less.

It should be noted that in the past the second-order theory has been considered difficult to apply. In some cases, this difficulty was due to the fact that source points were taken too close together in performing the solution, since the labor increases as the square of the number of points. At present, rules are being formulated for the maximum allowable spacing of the source points and a computing procedure is being devised which will make it possible for a person with no detailed knowledge of the theory to obtain solutions at the rate of about one a day (reference 3).

All of the above theory is restricted to bodies with pointed noses. For blunt-nosed bodies having detached shock waves at the tip, there is no adequate theory. Blunt bodies are of interest for two reasons: First, they have been proposed as necessary for adequate radar installation. Second, some of the mathematically derived optimum shapes have a small blunt region at the tip. Bodies in both of these categories, extremely blunt for radar and moderately blunt for optimization, have been investigated experimentally. The latter will be discussed first. Two mathematically derived optimum shapes of fineness ratio 3 are shown in figure 3. Both were optimized for a given length and base diameter, one by von Kármán by use of slender-body theory and one by Eggers and collaborators by use of hypersonic theory (reference 4). The bluntness at the tip is difficult to see except under magnification. Foredrag coefficients C_{D_F} of these shapes, based on frontal area, are presented in the figure as a function of Mach number and comparison is made with a cone and ogive of the same length and base diameter. The optimum bodies have about 15 percent less foredrag than the cone and about 35 percent less than the ogive. The incremental differences are of the order of a few hundredths in drag coefficient.

Elementary considerations indicate that drag reduction can be achieved with blunt tips in another way. If, for example, a cone of fineness ratio 3 is opened at the tip and a spherical tip inserted while the fineness ratio is held constant, there will be an increase in drag at the tip, but a decrease over the sides as a result of the decreased inclination of the sides to the stream. The increase at the tip occurs within a small frontal area whereas the decrease on the sides occurs over a large frontal area. The net effect on drag depends on the balancing of these opposite tendencies. This effect can be calculated by using experimental data for the foredrag of hemispheres and assuming that the side pressures will be the same as on a pointed cone of the same slope. The results of such a calculation are shown in figure 4, where increment of wave drag of the blunt shapes over that of the cone is plotted as a function of the ratio of tip radius to maximum radius for Mach numbers 1.5, 3, and 6. A small initial reduction in drag coefficient is indicated at all Mach numbers. The effect on these curves of the assumption that the side pressures remain conical is uncertain in the absence of experimental data. Therefore, the drag coefficients

SECURITY INFORMATION

of the family of bodies shown at the left in figure 5 were measured in the Ames supersonic free-flight wind tunnel (reference 5) and two of the experimental curves are shown. The bluntest shape in this family had a tip radius of 0.5 but the curves are extended toward an end point at a tip radius of 1 based on the best available values of the foredrag of a hemisphere. As can be seen by comparing, at a Mach number of 6, the calculated curve with experiment, the measured initial drag reduction is greater in both magnitude and extent than predicted so that favorable effect of the spherical tip on the side pressures is indicated. The comparison at a Mach number of 6 is typical of those obtained. The calculated curve is least quantitative in the region of the optimum bluntness. It is exact at either extreme of bluntness, zero or maximum, by definition. It is quantitatively useful for predicting the variation of drag with bluntness for tip radii greater than 0.5. The drag coefficients at the minimum points of these curves were lower than those of the cone by 0.01 to 0.02. The indicated optimum tip radius ranged from 0.2R at a Mach number of 1.5 to 0.1R at a Mach number of 6.

A second way of forming a family of blunt noses is to shorten progressively the parent shape, the pointed tip being replaced with a series of spherical tips of increasing diameter. Such a family was tested in free flight by the Langley Pilotless Aircraft Research Division (reference 6) and is shown in figure 5. In this case, no drag reduction due to opening the sides occurs since the sides are not disturbed. Nevertheless, the measurements show an initial decrease in drag coefficient. In this case, the skin friction changes in a manner favoring the blunter shapes, but this effect is too small to account for the drag improvement. Again, the indication is that reduction of the side pressures occurs in the presence of the spherical tip. The fact that this curve shows smaller drag penalties than the other two is a Mach number effect. At Mach numbers where the two sets of data overlap, the penalties are smaller for the first family than for the second as would be expected. Furthermore, there is some reason to suspect that, in the case of blunting by shortening, the drag minimum which exists at a Mach number of 1.2 would not occur at higher Mach numbers although the penalties would still be smaller than might be expected. It definitely appears, however, that for fixed values of the fineness ratio, the optimum shape at all supersonic Mach numbers will have a slightly blunt tip. Aside from the reduced drag, other advantages are associated with the blunt tip. The nose volume is greater for a given length and base diameter. A blunt nose has higher heat capacity at the tip than a pointed shape and is not so apt to burn off as a result of aerodynamic heating. A blunt nose is more rugged and less dangerous for handling in the field.

The abscissa scale of figure 5 extends out to a fully blunt hemispherical tip. The data in the right half of the figure apply, therefore, to noses suitable for radar. The incremental drag penalties at high bluntness are very severe, in the order of several tenths in drag

coefficient, and the severity increases with Mach number. The maximum
bluntness which can be used with zero penalty ranges from about 0.4 at
a Mach number of 1.2 to about 0.2 at a Mach number of 6. Some of the
noses represented in figure 5 are compared in figure 6 with some addi-
tional highly blunt shapes. Here, Mach number is the abscissa and the
increment in total drag coefficient over that of the pointed parent
shape is again the ordinate. Bodies carried over from the previous
slide include the blunted conical shapes with tip radii of 0.3 to 0.5,
and the blunted parabolic shapes with tip radii of 0.5, 0.7, and 0.8.
Additional shapes include a parabola of revolution, an ellipsoid, and

a shape defined by $\frac{y}{R} = \left(\frac{x}{l}\right)^{1/4}$. The additional data are from the Ames

10- by 14-inch and 1- by 3-foot supersonic wind tunnels. The Mach number
effect is surprisingly consistent for data collected from so many sources
for so many shapes. At Mach numbers below 2, the penalties diminish
rapidly until at a Mach number of 1.2 a 50-percent blunt nose is accept-
able. This reduction of penalty is due jointly to a rapid reduction in
hemispherical wave drag below Mach number 2 and a simultaneous increase
in the drag of the pointed shapes to which the penalties are referred.

In view of the severe drag penalties associated with large spherical
tips and the apparent desirability of the spherical tip for guidance pur-
poses, attention has recently been given to shielding the sphere aero-
dynamically. Three designs which have been proposed for use with infra-
red seekers are shown in figure 7 (reference 7). One is a conical-tipped
spike projecting in front of the sphere along the body axis. The second
is a slotted cone for which the slots comprise 50 percent of the frontal
area. The third is a quartz cone, made with 12 flat-sided triangular
elements in order to reduce distortion of the incoming radiation. In
the figure, the drag coefficients of these noses are compared with those
of the blunt shape desired for guidance and the pointed shape from which
the others were derived at Mach numbers between 1.0 and 1.8. The three
shielded noses have about the same drag and show substantial improvement
over the unshielded sphere. The improvement increases with increasing
Mach number. The choice between these three designs would be based on
considerations of guidance, structure, and simplicity. The drag-reducing
effectiveness of the spike at angle of attack has not been investigated.
The effects of spike length and diameter at Mach numbers near 2 have been
investigated by Moeckel (reference 8) at the Lewis Laboratory.

So far, the effect of fineness ratio on drag has not been discussed.
For severely blunt shapes, with tip radii equal to or greater than 0.5,
the effect of fineness ratio is small since the drag of the spherical
tip dominates the nose drag. However, for basically slender shapes, the
fineness ratio is an important variable as is shown in figure 8. In this
figure, the increment in foredrag, pressure plus friction, over that of
the same shape at fineness ratio 4 is plotted as a function of the fineness

ratio. These results were obtained from theory for cones and ogives (reference 9). A single curve can be faired reasonably well through data for both shapes at three Mach numbers: 2, 5, and 8. Two boundary-layer conditions are postulated, laminar flow at a Reynolds number of 5×10^6 representing a condition of low skin friction, and turbulent flow at a Reynolds number of 30×10^6 representing a typical high-friction condition. The two curves are nearly identical except that the high-friction curve shows a definite tendency to turn up at the extremes of fineness ratio plotted, whereas the low-friction curve continues down. These curves show relatively large drag changes with small changes in fineness ratio up to a fineness ratio of about 6. Beyond a fineness ratio of 6, the drag changes are smaller and other considerations might outweigh the drag improvement.

The final subject to be considered in this paper is the effect of body surface condition on the drag. This subject is one of great interest in connection with the mass production of missiles where perfect surfaces cannot be expected. Some data of this type are now available (reference 10) from flight tests of the RM-10 research vehicle at Mach numbers up to 2. The Reynolds numbers of the investigation were of the order of 50 million so that the boundary layers were predominantly turbulent. Several models with highly polished surfaces were tested to establish the drag coefficient for the smooth condition. The effect of roughness protruding from the surface was investigated with a body thickly coated with 0.01-inch-diameter sand particles. This dimension can be compared with the maximum body radius which was 3 inches. A second model was made to simulate a partly ground aluminum casting. Its surface was about 70 percent smooth, the remainder being pitted below the level at which grinding was stopped. Although the pits were only about 0.002 inch deep, the model looked and felt rough. The effect of longitudinal waves, such as might occur in the manufacture of metal bodies by the spinning technique, was investigated with a third model having waves about 0.02 inch deep and about 0.5 inch long extending over the entire length. The results of these tests are shown in figure 9. It will be noted that neither the wavy surface nor the pitted surface of the simulated casting caused any measurable increase in drag. The sand-coated surface, however, increased the drag substantially. It was established that this drag change was not a change in base drag. It appears from these exploratory tests that, at very high Reynolds numbers at which the boundary layers are naturally turbulent, some degree of surface roughness due to pitting or waviness can be tolerated but that roughness projecting from the surface can cause substantial drag increases.

In summary, it appears that the nose of minimum drag for a given fineness ratio will have a slightly blunt tip at all supersonic Mach numbers. For noses with spherical tips, the optimum tip radius varies from 0.1 to 0.2 of the maximum radius depending on the Mach number. Tip radii twice the optimum can be tolerated without increasing the drag over that

of the pointed parent shape. Beyond this bluntness, severe drag penalties
occur which increase with increasing Mach number. Only semiempirical
methods exist for calculating the drag of these shapes. The theory for
pointed shapes seems adequate, since reasonably accurate estimates of
pressures and pressure drag can now be obtained for most of the Mach
numbers and fineness ratios of current interest.

REFERENCES

1. Van Dyke, Milton D.: A Study of Second-Order Supersonic-Flow Theory.
     NACA TN 2200, 1951.

2. Eggers, Alfred J., Jr., and Savin, Raymond C.: Approximate Solutions
     to the Flow About Nonlifting Bodies of Revolution at High Supersonic
     Air Speeds. (Prospective NACA paper)

3. Van Dyke, Milton D.: Practical Calculation of Second-Order Supersonic
     Flows past Bodies of Revolution. (Prospective NACA paper)

4. Eggers, Alfred J., Jr., Dennis, David H., and Resnikoff, Meyer M.:
     Minimum Drag Bodies of Revolution at High Supersonic Air Speeds.
     (Prospective NACA paper)

5. Sommer, Simon C., and Stark, James A.: The Effect of Bluntness on the
     Drag of Spherical-Tipped Truncated Cones at Mach Numbers Between 1.5
     and 7. (Prospective NACA paper)

6. Hart, Roger G.: Flight Investigation of the Drag of Round-Nosed Bodies
     of Revolution at Mach Numbers from 0.6 to 1.5 Using Rocket-Propelled
     Test Vehicles. NACA RM L51E25, 1951.

7. Piland, R. O.: Free-Flight Investigation of the Drag Penalties of
     Several Missile Nose Shapes Suitable for Infra-Red Seeking Devices.
     (Prospective NACA paper)

8. Moeckel, W. E.: Flow Separation ahead of a Blunt Axially-Symmetric
     Body at Mach Numbers 1.76 to 2.1. (Prospective NACA paper)

9. Rossow, Vernon J.: Applicability of the Hypersonic Similarity Rule
     to Pressure Distributions Which Include the Effects of Rotation
     for Bodies of Revolution at Zero Angle of Attack. NACA TN 2399,
     1951.

10. Jackson, H. H.: Flight Measurements of the Effect of Surface Condition
     on the Transonic and Supersonic Drag of Fin-Stabilized Parabolic
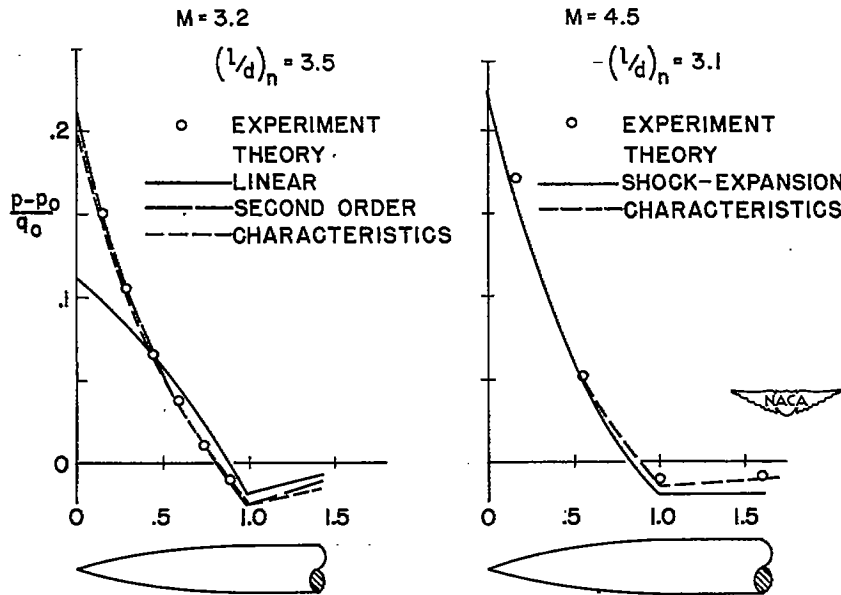   Bodies of Revolution. (Prospective NACA paper)

M = 3.2

$\left(\frac{1}{d}\right)_n = 3.5$

o   EXPERIMENT
    THEORY
    ————LINEAR
    —·—·—SECOND ORDER
    —————CHARACTERISTICS

$\frac{p-p_0}{q_0}$

.2

.1

0

0   .5   1.0   1.5

M = 4.5

$-\left(\frac{1}{d}\right)_n = 3.1$

o   EXPERIMENT
    THEORY
    ————SHOCK-EXPANSION
    —————CHARACTERISTICS

0   .5   1.0   1.5

Figure 1.- Comparison of approximate theories with characteristics solutions and experimental data.

·20

10

0

DRAG −10
ERROR,
%   −20

−30

−40

−50

SECOND-ORDER
OGIVES   CONES

OGIVES   CONES
SHOCK EXPANSION

OGIVES CONES
LINEARIZED

0   0.5   1.0   1.5   2.0

HYPERSONIC SIMILARITY PARAMETER, $K = \frac{M}{\frac{1}{d}}$
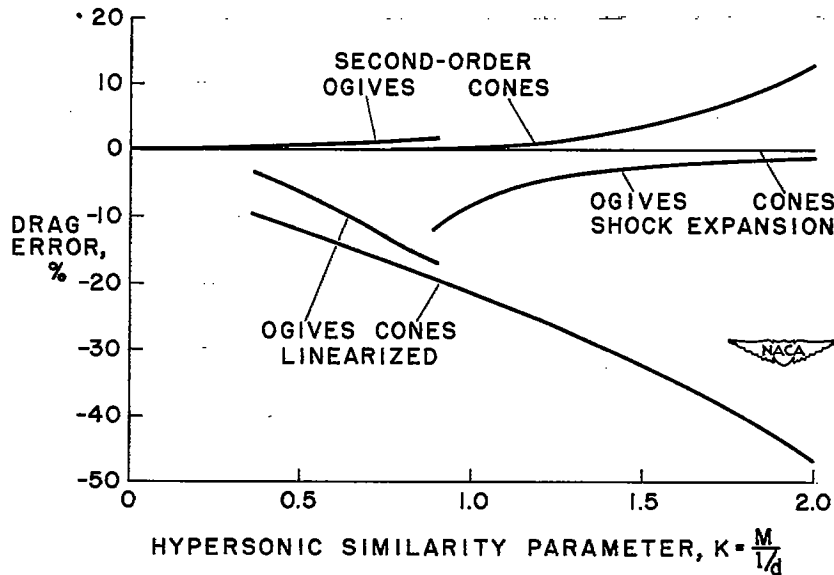
Figure 2.- The drag errors of three approximate theories as a function of the hypersonic similarity parameter.
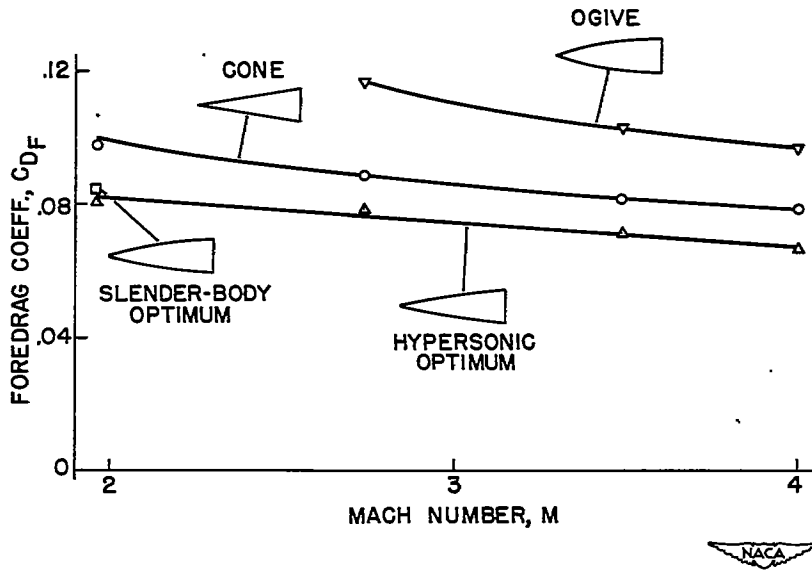
Figure 3.- Foredrag coefficients of two optimum shapes compared with a cone and tangent ogive of the same length and base diameter.
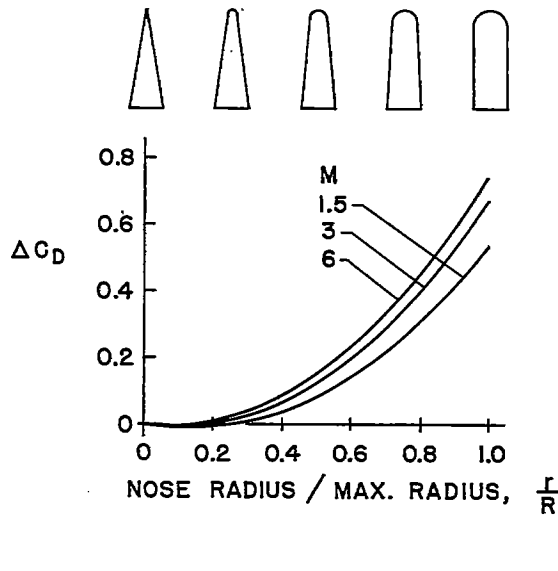
Figure 4.- The calculated variation with tip radius of the drag increment due to bluntness for truncated conical noses with spherical tips.
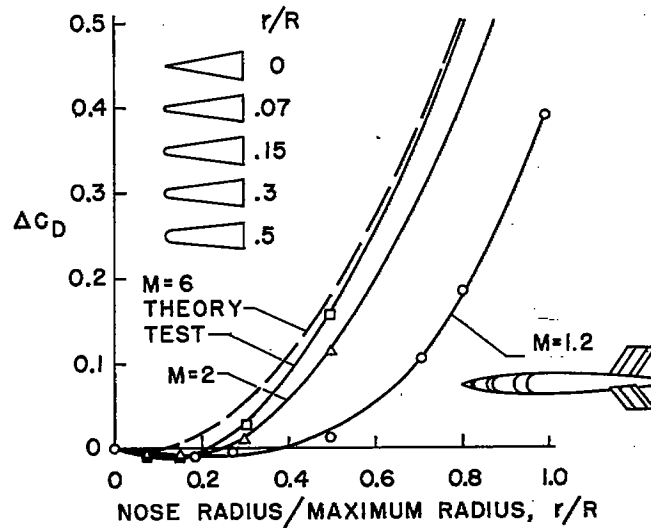
Figure 5.- The experimental variation with tip radius of the drag incre-
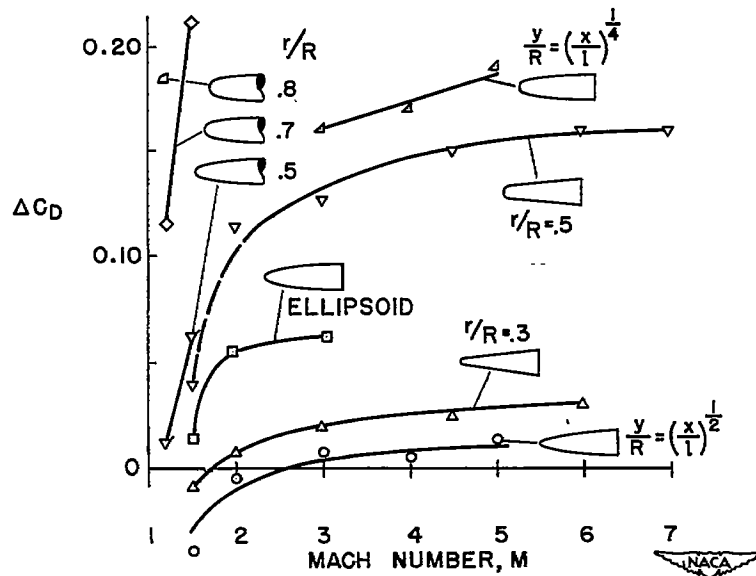ment due to bluntness for two families of shapes.

Figure 6.- Dependence on Mach number of the drag penalty due to bluntness.
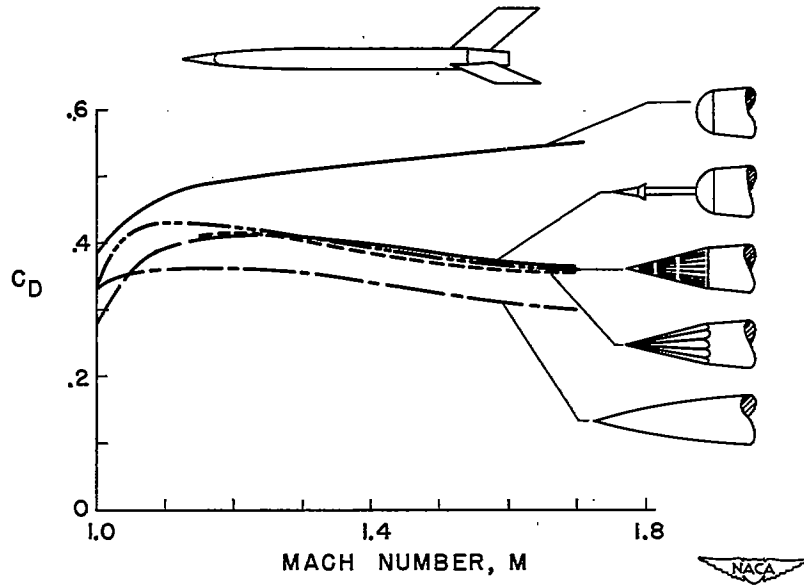
Figure 7.- Use of a projecting spike or slotted cone to reduce the drag
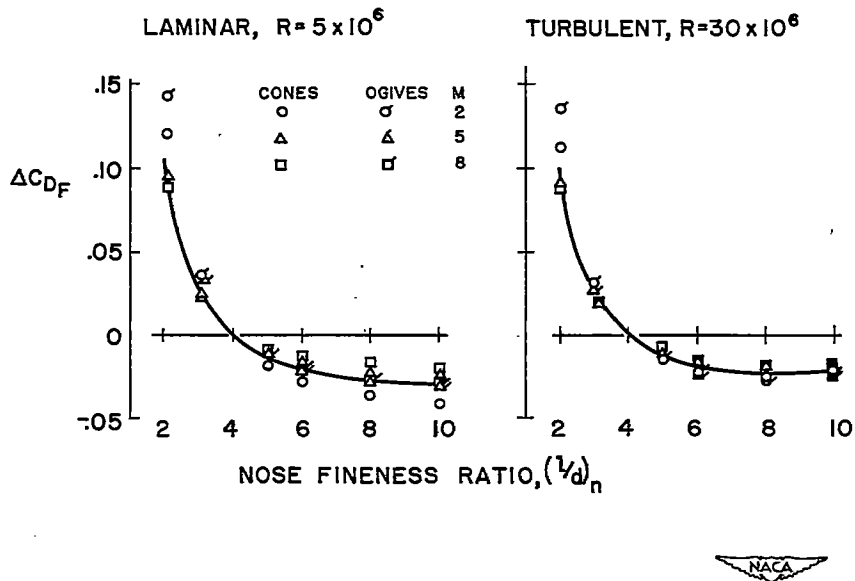of a spherical-tipped infra-red seeker.

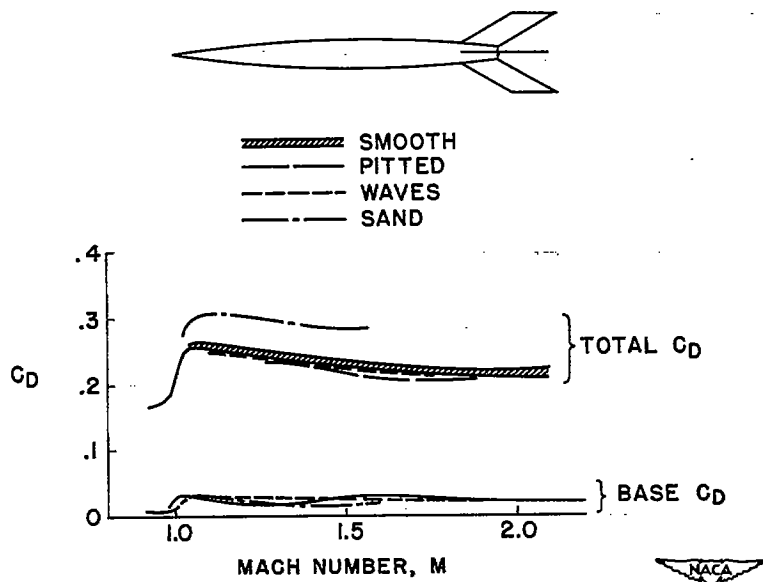Figure 8.- The effect of fineness ratio on foredrag for cones and ogives.

Figure 9.- The effect at very high Reynolds numbers of three kinds of
surface imperfections on the drag.

BASE PRESSURE ON WINGS AND BODIES

WITH TURBULENT BOUNDARY LAYERS[1]

By Dean R. Chapman
Ames Aeronautical Laboratory

At present there is no satisfactory theory for calculating the pressure which acts at the blunt base of an object traveling at supersonic velocity. In fact, the essential mechanism determining the base pressure is only imperfectly understood. As a result, the existing knowledge of base pressure is based almost entirely on experiments. The main object of this paper is to summarize the principal results of the many wind-tunnel and free-flight measurements of base pressure on both bodies of revolution and blunt-trailing-edge airfoils. A relatively simple method of estimating base pressure is presented, and an indication is given as to how the characteristics of base pressure play an essential role in determining the shape of an aerodynamically efficient object for supersonic flight.

It now is generally accepted that the base pressure depends markedly on the type of boundary-layer flow, that is, whether laminar or turbulent. Although extensive measurements have been made at the Ames Laboratory and in various other laboratories with both types of boundary-layer flow, only the case of turbulent flow will be considered here. Such a choice is made, of course, because turbulent flow at present is of more practical importance to the missile designer than is laminar flow.

The number of variables that affect base pressure are many, since anything that affects the boundary-layer flow can affect the base pressure. It will be convenient, however, to think of each variable that affects base pressure as acting in one or more of three ways: first, by changing the flow field exterior to the boundary layer - such changes affect the base pressure in a manner that can be estimated from considerations of the flow of an inviscid gas; second, by changing the thickness of the boundary layer just upstream of the base - this latter type of change affects base pressure in a manner that can be determined by systematic experiments; and third, by changing the distribution of velocity and density within the boundary layer, or within the mixing layer downstream of the base. This last type of effect is complicated indeed and has thus far proven intractable by theoretical methods.

The chief variable of the first type mentioned is body shape. Even in an inviscid flow, base pressure depends on the body shape because the local pressure and local Mach number approaching the base is different for different bodies. The upper sketch in figure 1 illustrates the flow about a given body; the lower sketch in this figure illustrates a

---

[1]This is a reprint of the paper by the same author which was presented at the NACA Conference on Aerodynamic Design Problems of Supersonic Guided Missiles at the Ames Aeronautical Laboratory on Oct. 2-3, 1951.

fictitious inviscid flow from which the pertinent Mach number and static pressure of the disturbance field can be calculated. The notation is as follows: M_∞ and p_∞ designate the free-stream Mach number and static pressure, respectively; whereas, M' and p' designate the Mach number and static pressure induced in the vicinity of the base by the presence of the body. As is illustrated, M' and p' represent conditions along a hypothetical extension, averaged over a region occupying the same relative streamwise position as the dead-air region in the real flow. The surface of the hypothetical extension is parallel to the free-stream direction. The significance of M' and p' evaluated in this particular manner, is that they form reference quantities to which the base pressure can be referred and be nearly independent of profile shape in an inviscid flow. In a real flow, therefore, the quantities M' and p' can be thought of as the Mach number and static pressure corrected for the effect of body shape on the flow field exterior to the boundary layer. The method illustrated is valid for small boattail angles only.

Since M' and p' are used extensively in subsequent figures, it may be of some help in clarifying the basic idea by mentioning an analogy, namely, the theory of subsonic wind-tunnel-wall corrections. There, the free-stream Mach number and pressure are corrected for the disturbance induced in the vicinity of the model by the presence of the tunnel walls. Here, the same quantities are corrected for the disturbance induced in the vicinity of the base by the presence of the body. In both cases, the correction is accurate only if the disturbance field is small and is nearly uniform over the region in question.

In general, numerical calculations of M' and p' show that as far as base pressure is concerned this correction is significant at all supersonic Mach numbers for bodies of revolution with boattailing. For bodies without boattailing, the correction is less important. For airfoils the correction is important at low-supersonic Mach numbers where the bow wave is detached, but is negligible at moderate Mach numbers where the bow wave is attached. In most cases the static-pressure correction is larger than the Mach number correction.

In the examples presented later, the quantities M' and p' for cone-cylinder bodies of revolution have been determined from the characteristics solutions of reference 1. For bodies of revolution with curved sides, M' and p' have been calculated from the second-order theory of Van Dyke (reference 2). The corresponding quantities for airfoils in the region of bow wave detachment have been determined from the results of Guderley and Yoshihara (reference 3) and of Vincenti and Wagoner (reference 4).

The principal use to be made of the quantities M' and p' is in estimating the base pressure of a boattailed profile from a knowledge of the base pressure on a profile without boattailing. The essential

concept involved is that the base pressure, when referred to M'
and p', is independent of body shape. This concept neglects changes
in the boundary-layer flow. Figure 2 illustrates the accuracy of esti-
mating base pressure in this manner. Afterbodies converging toward the
base are designated by positive boattail angles and are plotted on the
right of the ordinate axis. Cones are designated by negative boattail
angles and are plotted on the left. The line composed of short dashes
represents the estimated values from calculations of M' and p'. The
line composed of long dashes represents a method of estimation recently
given by Cortright and Schroeder (reference 5). In this and most subse-
quent figures, the base pressure ratio is plotted as the ordinate; hence,
it is to be remembered that the base drag per unit base area is propor-
tional to one minus the ordinate, and that the base drag is reduced if
the base pressure is increased. In figure 2, for example, it is seen
that at a Mach number of 1.5 the observed increase in base pressure is
such that the base drag is reduced almost to zero at boattail angles of
about 15°. It is seen further that, in the range shown, negative boat-
tail angles on bodies of revolution lower the base pressure, thus
increasing the base drag considerably, whereas positive boattail angles
have the opposite effect.

Figure 3 shows the effect of boattail angle on the base pressure of
airfoils. It is evident that there is little effect of boattail angle
in this latter case. This is in accordance with the estimate based on
the calculated values of M' and p', as indicated by the short dashes.
In view of the reasonable agreement between these experiments and the
estimated values, it is believed that for turbulent boundary-layer flow
the effect of boattailing on base pressure is due principally to changes
in the outer flow field rather than to changes in boundary-layer flow
brought about by the boattailing.

When employing the above method of estimating base pressure it is
necessary, as already mentioned, to have experimental data on a profile
without boattailing. The compiling of such data is greatly simplified
by the fact that the effect of Reynolds number on base pressure is small
for turbulent boundary-layer flow and often can be neglected. This is
illustrated by figure 4 showing base pressure measurements as a function
of Reynolds number for various profile shapes, with and without boat-
tailing, and for several different Mach numbers.

For airfoils with turbulent boundary-layer flow, the effect of
Reynolds number also is small, as indicated in figure 5. From a com-
parison of figures 4 and 5, it can be concluded that, in general, moder-
ate differences in Reynolds number will have only a small effect on base
pressure if the boundary layer is turbulent. Therefore, the many experi-
mental measurements of base pressure for which the test Mach numbers and
Reynolds numbers both varied can be plotted as a function only of the
Mach number. Such a plot for a number of bodies of revolution without

boattailing is shown in figure 6. Also shown in this figure are data
for several cones since these latter data (unpublished data from Ames
supersonic free-flight wind tunnel) are the only data available which
are representative of turbulent flow at Mach numbers near 6. These
data for cones can be compared directly with the other data since M'
and p' are used as reference quantities in this figure. It is to be
noted that data from a number of different laboratories (references 6
to 11, plus unpublished data of the Ames 10- by 14-inch supersonic wind
tunnel) are included here; the free-flight measurements are designated
by filled symbols and wind-tunnel measurements, which were taken with
rear sting supports, are designated by open symbols. Considering the
wide variety of experimental techniques employed in obtaining these
data, the degree of mutual agreement is regarded as satisfactory. The
mean curve passed through these data can be used either to estimate the
base pressure of a boattailed body according to the method described
earlier, or, if a body has no boattailing and a cylinder three or four
diameters long preceding the base, then this mean curve can be used
directly to give the base pressure. The equation used in estimating the
base pressure of a given body, for which M' and p' have been calcu-
lated, is

$$\frac{p_b}{p_\infty} = \left(\frac{p_b}{p'}\right)_{M'} \frac{p'}{p_\infty}$$

where the quantity $\left(p_b/p'\right)_{M'}$ is the experimental value of p_b/p'
picked from the curve of figure 6 at the Mach number M'.

Of course, a plot similar to the one shown can also be made for air-
foils. Such a plot is presented in figure 7, where again free-flight
data (reference 12) are represented by filled symbols and wind-tunnel
data (reference 13 and unpublished data from the Langley 9- by 12-inch
supersonic blowdown tunnel, the Langley 9-inch supersonic tunnel, and
the Ames 1- by 3-foot wind tunnels) are represented by open symbols.
Most of these data represent measurements on finite-span wings on which
considerable spanwise variations in base pressure can exist. In such
cases, the values shown represent an average over the span of the
trailing edge. The filled point situated at the extreme left in this
figure actually was taken at a flight Mach number of 1.0, but, on this
graph, it plots in the position shown because of the large effect of
profile shape on base pressure in the region of bow wave detachment.
All these data for airfoils were obtained with the trailing edge normal
to the stream direction. Rectangular plan forms were used for most
measurements, although one set, indicated by the tagged symbols, was
obtained with a triangular wing. The base pressure for the two different
plan forms is nearly the same. Some base pressure measurements recently

have been obtained at the Langley Laboratory on a constant-chord wing
with trailing edge swept back 45°. These latter measurements are not
shown in figure 7 because of the difficulty in calculating the average
value of p' for a sweptback wing. The actual measured values of the
base pressure, however, were nearly the same as for unswept wings at
1.62 Mach number, but were about 20- to 50-percent higher at Mach num-
bers of 1.41 and 1.96.

A comparison of figures 6 and 7 shows that, at high-supersonic Mach
numbers, the base pressure on bodies and airfoils is almost the same,
with the base pressure in each case approaching a vacuum as the Mach
number is increased. On the other hand, it can be seen also that at
low-supersonic Mach numbers the base pressure is much lower for airfoils
than bodies. In fact, at a Mach number of 1.2, the observed difference
is such that the base drag per unit base area of an airfoil is over two
times that of a body of revolution. The characteristics just noted,
namely, the essential difference in base pressure between bodies and
airfoils at low-supersonic Mach numbers, and the essential similarity
at high-supersonic Mach numbers where the base pressure approaches zero,
would exist in an inviscid flow (reference 8), and hence these charac-
teristics are believed to be associated to a large degree with the
behavior of the flow exterior to the boundary layer.

All data in figures 6 and 7 represent conditions where the turbu-
lent boundary layer is thin relative to the base dimension. If the
boundary layer is thick compared to the base height, then the base pres-
sure will be somewhat higher, and the base drag correspondingly lower.
A general trend of increasing base pressure with increasing boundary-
layer thickness has been found in the experiments on bodies (reference 8)
and airfoils (unpublished) conducted at the Ames Laboratory. Another
general trend, of increasing base pressure with increasing surface tem-
perature, has been observed by Kurzweg at the Naval Ordnance Laboratory
(reference 7). Since an increase in surface temperature also increases
the boundary-layer thickness, both trends can be shown together by
plotting base pressure against a parameter proportional to the ratio of
turbulent boundary-layer thickness to base thickness. Such a parameter,
as indicated in figure 8, involves the ratio of body length to base
diameter, the Reynolds number, and the ratio $\delta/(\delta$ no heat). This
latter factor represents the ratio of boundary-layer thickness of a
heated body to that of an unheated body at the same Reynolds number and
has been determined from the analysis of the turbulent boundary layer
with heat transfer as given by Van Driest (reference 14). The open
symbols, which represent the experiments at the Ames Laboratory on bodies
without heat transfer, show a slow rise in base pressure as the boundary-
layer thickness increases.

The filled symbols, which represent the experiments at the Naval
Ordnance Laboratory on heated bodies, show a much more rapid rise in

base pressure. It is evident, then, that the transfer of heat affects the base pressure principally through the changes it brings about in the distribution of density and velocity within the boundary layer, rather than through the changes it brings about in boundary-layer thickness.

For airfoils, the ratios of boundary layer to base thickness that are of practical interest extend to considerably higher values than for bodies of revolution. As a result, the boundary-layer thickness has to be considered more carefully in estimating base pressure. This is illustrated in figure 9 where the base pressure (unpublished data from Ames 1- by 3-foot supersonic wind tunnels) is plotted as a function of the parameter which is approximately proportional to the ratio of turbulent boundary-layer thickness to trailing-edge thickness. The airfoil thickness ratio t/c and the trailing-edge bluntness ratio h/t were systematically varied in these experiments. The results shown represent twelve different profiles and correlate reasonably well on this plot. From this it can be seen, for example, that a thin airfoil with a thin trailing edge will have a significantly higher base pressure than a thick airfoil with a fully blunt trailing edge. It should be mentioned that although only a small effect of Reynolds number was noted earlier, a significant effect of boundary-layer thickness is noted in figure 9 because the fifth root of the Reynolds number is involved in this latter figure.

The extent to which the characteristics of base pressure influence the total afterbody drag of bodies of revolution is illustrated in figure 10. Here the afterbody length is held constant and the base diameter varied. In these examples the side drag has been calculated on the assumption of inviscid flow, and the base drag has been estimated by the method described earlier. A few experimental points also are shown in figure 10. It can be seen that at a Mach number of 1.5, the afterbody drag in this particular example is reduced about 30 percent by boattailing to a base diameter of about two-thirds of the body diameter. The minimum afterbody drag occurs when the base drag is about one-fifth of the total afterbody drag. At a Mach number of 3 the situation is about the same; but at a Mach number of 8 there is seen to be no significant effect of afterbody shape on the total afterbody drag. Hence, at very high supersonic Mach numbers, there is little to gain by boattailing.

The characteristics of base pressure also have an important effect on the drag of airfoils. This is illustrated in figure 11, where the calculated pressure drag of a family of airfoils, all having the same cross-section area, is plotted as a function of the ratio of trailing-edge thickness to maximum airfoil thickness. For each value of the trailing-edge thickness, the profile ahead of the base was determined by the condition that the foredrag calculated from shock-expansion theory be a minimum. The base drag was determined from the correlated

measurements presented earlier except in the case of a Mach number of 8
for which the base pressure was assumed to be zero. It is apparent
that, at Mach numbers of 1.5 and 3, the minimum total pressure drag
occurs for airfoils with a slightly blunt trailing edge. Also, at these
Mach numbers a substantial drag penalty will occur if a fully blunt
trailing edge is employed instead of the optimum. At a Mach number of 8,
however, the drag penalty compared to the optimum is small even with a
vacuum at the base; the minimum pressure drag at this Mach number occurs
when the trailing-edge thickness is about two-thirds of the maximum air-
foil thickness. The main practical significance of these results lies
in the structural advantages of a thick trailing edge, particularly when
a control surface is employed, since the thickness of the airfoil at the
hinge line and the torsional stiffness of the control surface are greatly
increased.

From the viewpoint of increasing missile performance, it naturally
is desirable to be able to reduce the base drag. One method of doing this
has been indicated by Cortright and Schroeder of the Lewis Laboratory
(reference 15). They found that by permitting small quantities of air to
flow out of the base of bodies of revolution the base pressure could be
increased a substantial amount. Some of their results are presented in
figure 12 where the measured base pressure is plotted as a function of
the ratio of jet chamber pressure $\left(p_j\right)$ to free-stream static pressure.
One curve is for a body without boattailing, and the other is for a body
with a 9.3° boattail angle. The observed maximum increase in base pres-
sure, as indicated in figure 12, corresponds to a decrease in base drag
of about 30 and 60 percent, respectively. The quantity of bleed air
required at the optimum value of jet pressure for the body without boat-
tailing corresponds to a mass flow of bleed air equal to about 4 percent
of the mass flow that would flow through the base if the free stream
passed through the base undisturbed.

Figure 13 shows that the base drag of airfoils also can be reduced
considerably by bleeding air out of the base. (These latter unpublished
data for airfoils were obtained in the Ames 1- by 3-foot wind tunnels.)
At Mach numbers of 1.45 to 2, the observed maximum increases in base
pressure correspond to base drag reductions of about 36 and 35 percent,
respectively. In these two cases the jet exit area is 18 percent of the
total base area, and the optimum values of jet pressure correspond to a
mass flow of bleed air between about 3 and 5 percent of the mass flow
that would flow through the base if the free stream passed through the
base undisturbed. Also, in these two cases the optimum jet pressures
correspond to jet-exit Mach numbers in the high-subsonic region.

In a comparison of figures 12 and 13, it is significant to note
that the optimum jet pressure in all cases is less than the free-stream
static pressure since this greatly minimizes the problem of supplying
bleed air.

All preceding results are for bodies of revolution and blunt trailing-edge airfoils set at zero angle of attack. In figure 14 some typical data for bodies of revolution (references 10, 16, and unpublished data from the Lewis 1- by 1-foot and Ames 1- by 3-foot wind tunnels) are collected which illustrate the effect of angle of attack on base pressure. In each case the base pressure decreases considerably as the angle of attack is increased. To what extent this decrease is due to changes in the exterior flow in the vicinity of the base and to what extent it is due to the changes in boundary-layer flow approaching the base is not known as yet. The situation is considerably clearer for airfoils, since the characteristics of the exterior flow at angle of attack can be calculated easily. The calculated values of M' and p' for airfoils do not change with small changes in angle of attack. It is not surprising, therefore, that over the Mach number region shown the base pressure on airfoils, as indicated in figure 15, does not change significantly with a change in angle of attack. This result is seen to apply at Mach numbers ranging from 1.5 to 4.0, and for a variety of airfoil sections. Comparing these two figures, we see that the situation is quite similar to that noted earlier when considering the effect of boattail angle on base pressure. The observed effect is large for bodies of revolution but small for airfoils.

Some measurements at angle of attack have been made on a 45° sweptback blunt trailing edge (unpublished data from Langley 9- by 12-inch supersonic blowdown tunnel) which indicate that up to about 10° the effect of angle of attack on base pressure is small at 1.96 Mach number, but is sizable at 1.62 and 1.41 Mach number at which the bow wave is detached.

The results of this paper can be summarized in three general statements: First, base drag of bodies of revolution and airfoils can be estimated with reasonable accuracy from the correlation of experiments and from the method of calculation described at the beginning of this paper; second, a body of revolution or an airfoil that is designed to have minimum drag at supersonic speeds generally will not be pointed at the rear, but will have a finite base, the thickness of which generally increases as the Mach number increases; and third, some recent experiments have indicated that the base drag of bodies of revolution and airfoils can be significantly reduced by bleeding relatively small quantities of air out of the base.

REFERENCES

1. Clippinger, R. F., Giese, J. H., and Carter, W. C.: Tables of Supersonic Flows about Cone Cylinders. Part I: Surface Data. Rep. No. 729, Ballistic Res. Lab., Aberdeen Proving Ground, 1950.

2. Van Dyke, Milton D.: First- and Second-Order Theory of Supersonic Flow past Bodies of Revolution. Jour. Aero. Sci.; vol. 18, no. 3, March 1951, pp. 161-178.

3. Guderley, G., and Yoshihara, H.: The Flow over a Wedge Profile at Mach Number 1. Jour. Aero. Sci., vol. 17, no. 11, Nov. 1950, pp. 723-735.

4. Vincenti, Walter G., and Wagoner, Cleo B.: Transonic Flow past a Wedge Profile with Detached Bow Wave - General Analytical Method and Final Calculated Results. NACA TN 2339, 1951.

5. Cortright, Edgar M., Jr., and Schroeder, Albert H.: Investigation at Mach Number 1.91 of Side and Base Pressure Distributions over Conical Boattails without and with Flow Issuing from Base. NACA RM E51F26, 1951.

6. Charters, A. C., and Turetsky, R. A.: Determination of Base Pressure from Free-Flight Data. Rep. No. 653, Ballistic Res. Lab., Aberdeen Proving Ground, 1948.

7. Kurzweg, H. H.: New Experimental Investigations on Base Pressure in the NOL Supersonic Wind Tunnels at Mach Numbers 1.2 to 4.24. Naval Ordnance Lab. Memo. 10113, Jan. 23, 1950.

8. Chapman, Dean R.: An Analysis of Base Pressure at Supersonic Velocities and Comparison with Experiment. NACA TN 2137, 1950.

9. Peck, Robert .F.: Flight Measurements of Base Pressure on Bodies of Revolution with and without Simulated Rocket Chambers. NACA RM L50I28a, 1950.

10. Cohen, Robert J.: Aerodynamic Characteristics of Four Bodies of Revolution Showing Some Effects of Afterbody Shape and Fineness Ratio at Free-Stream Mach Numbers from 1.50 to 1.99. NACA RM E51C06, 1951.

11. Bogdonoff, Seymour M.: A Preliminary Study of Reynolds Number Effects on Base Pressure at $M = 2.95$. Rep. No. 182, Princeton Univ., Aero. Eng. Lab., June 12, 1951.

12. Morrow, John D., and Katz, Ellis: Flight Investigation at Mach
       Numbers from 0.6 to 1.7 to Determine Drag and Base Pressures on
       a Blunt-Trailing-Edge Airfoil and Drag of Diamond and Circular-Arc
       Airfoils at Zero Lift. NACA RM L50E19a, 1950.

13. Beastall, D., and Eggink, H.: Some Experiments on Breakaway in
       Supersonic Flow (Part II). TN No. Aero. 2061, British R.A.E.,
       June 1950.

14. Van Driest, E. R.: Turbulent Boundary Layer in Compressible Fluids.
       Jour. Aero. Sci., vol. 18, no. 3, March 1951, pp. 145-160, 216.

15. Cortright, Edgar M., Jr., and Schroeder, Albert H.: Preliminary
       Investigation of Effectiveness of Base Bleed in Reducing Drag of
       Blunt-Base Bodies in Supersonic Stream. NACA RM E51A26, 1951.

16. Esenwein, Fred T., Obery, Leonard J., and Schuller, Carl F.: Aero-
       dynamic Characteristics of NACA RM-10 Missile in 8- by 6-Foot
       Supersonic Wind Tunnel at Mach Numbers from 1.49 to 1.98. II -
       Presentation and Analysis of Force Measurements. NACA RM E50D28,
       1950.

DISTURBANCE INDUCED NEAR BASE BY PRESENCE OF BODY

METHOD OF DETERMINING M′ AND p′
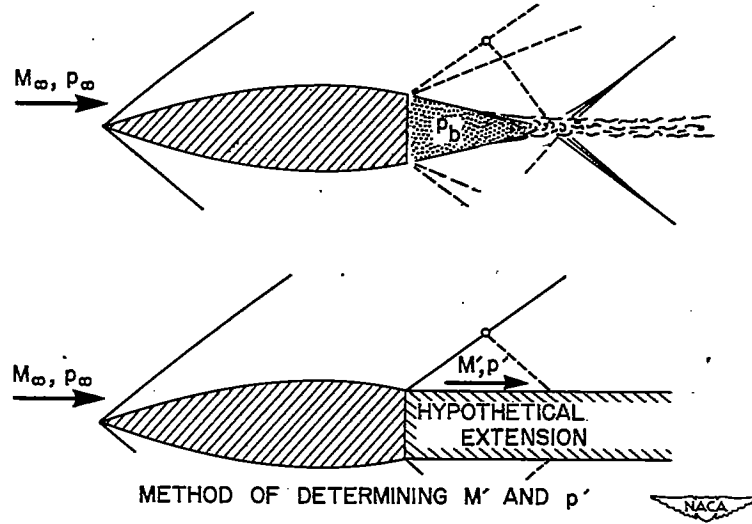
Figure 1

BODIES

EFFECT OF BOATTAIL ANGLE ON BASE PRESSURE
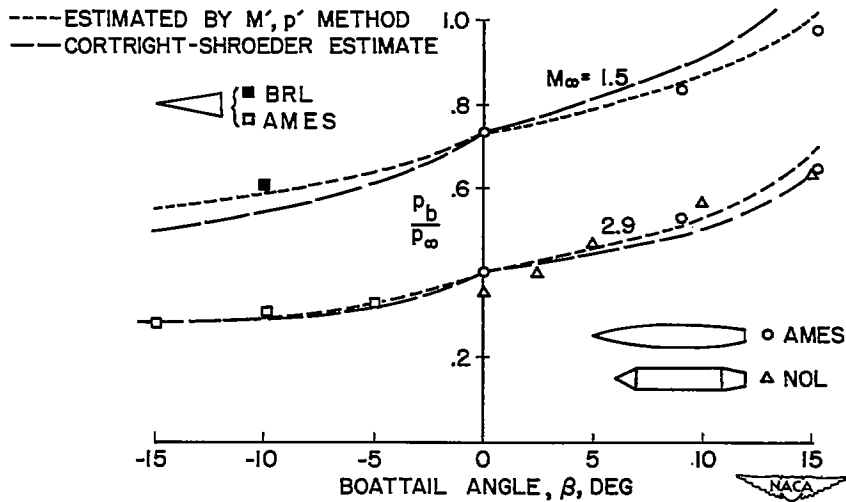
Figure 2

AIRFOILS
EFFECT OF BOATTAIL ANGLE ON BASE PRESSURE
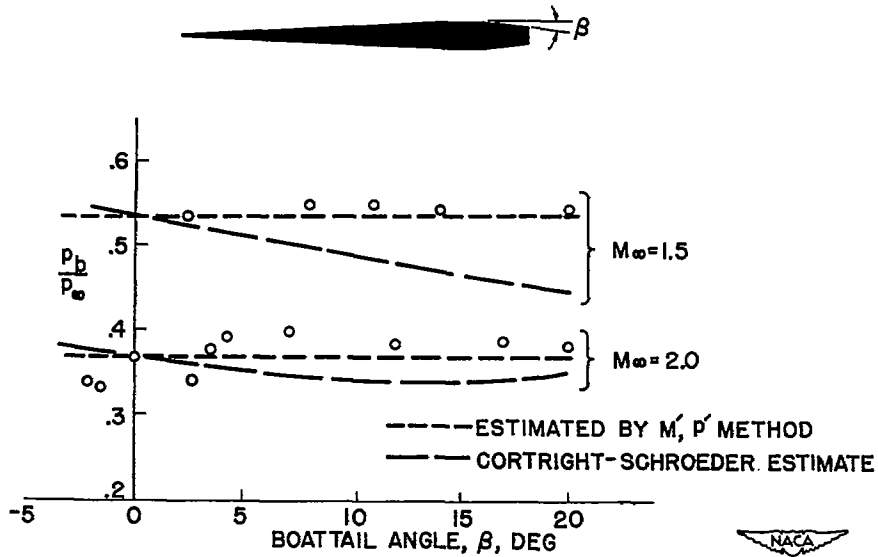
Figure 3

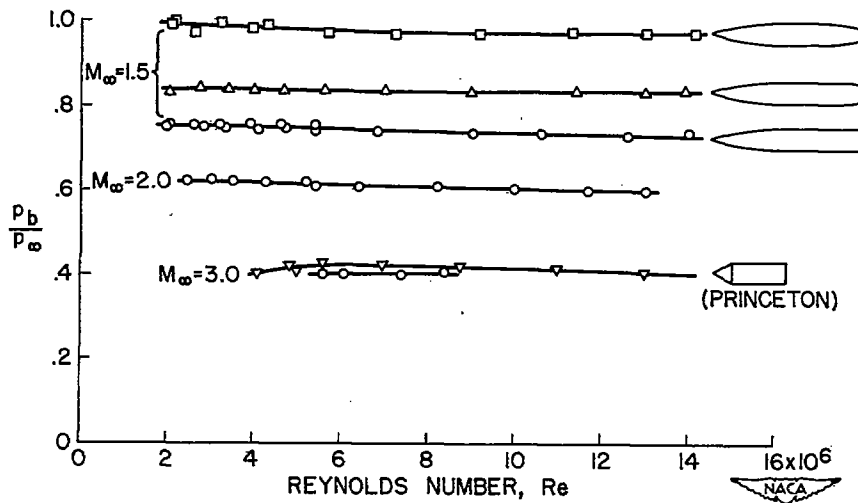## BODIES
REYNOLDS NUMBER EFFECT ON BASE PRESSURE

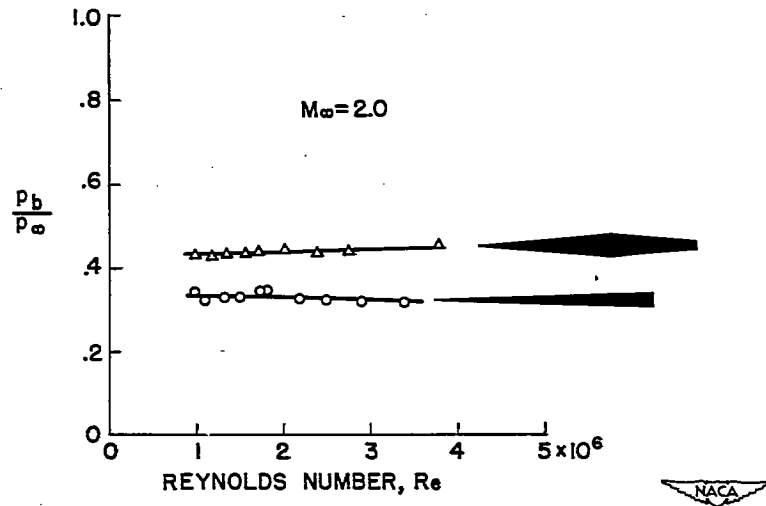Figure 4

AIRFOILS
REYNOLDS NUMBER EFFECT ON BASE PRESSURE

$M_\infty = 2.0$

$\dfrac{p_b}{p_\infty}$

REYNOLDS NUMBER, Re

Figure 5

BODIES
BASE PRESSURE VERSUS MACH NUMBER

FREE-FLIGHT DATA

- ● LANGLEY PARD
- ▲ AMES SSFF
- ■ BRL
- ▼ BRL
- ◆ AMES SSFF

WIND-TUNNEL DATA

- ○ AMES 10x14-IN.
- △ LEWIS 6x8-FT.
- □ AMES 1x3-FT.
- ▽ NOL
- ◇ AMES 1x3-FT.
- ◁ AMES 10x14-IN.
- ◁ PRINCETON

$\dfrac{p_b}{p'}$

M'
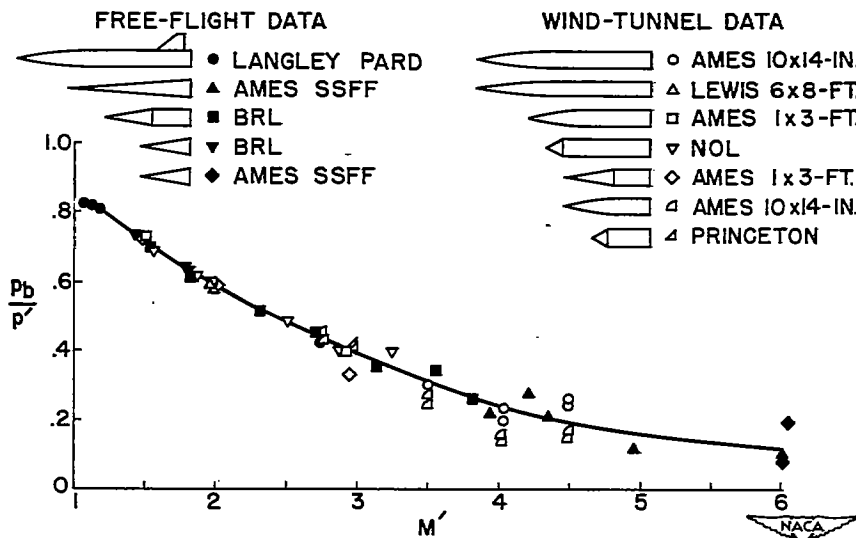
Figure 6

AIRFOILS
BASE PRESSURE VERSUS MACH NUMBER

PROFILE		DATA SOURCE	PLANFORM
●	LANGLEY, PARD	RECT., $R = 2.7$
△		
□	} AMES 1x3-FT.	RECT., $R = 3$
▽		
◇	} LANGLEY, 9 x 12 IN	RECT., $R = 2.7$
⊠		DELTA, $R = 4$
◁	LANGLEY, 9 IN	TWO DIMEN.
◻	NPL ENGLAND (HALF-MODEL)	TWO DIMEN.

$\dfrac{p_b}{p'}$

M'
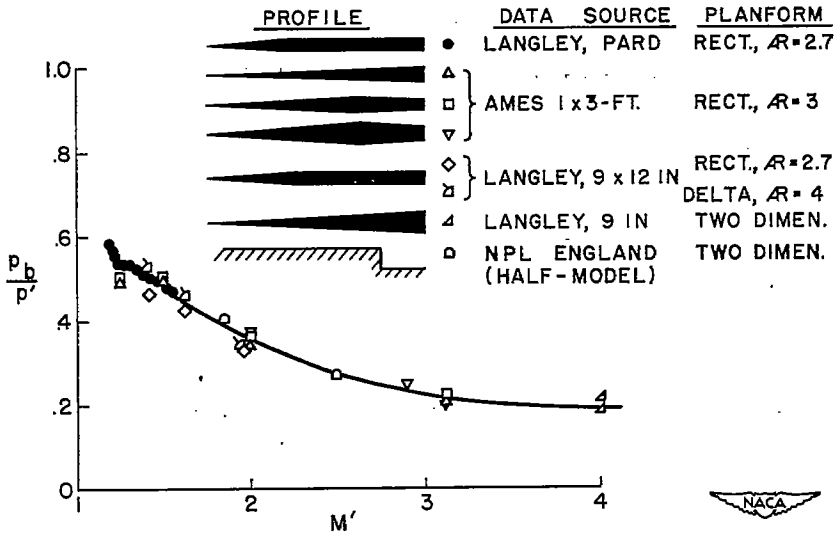
Figure 7

BODIES
BASE PRESSURE VERSUS RATIO OF BOUNDARY-LAYER
THICKNESS TO BASE HEIGHT

$\dfrac{p_b}{p'}$

M'=1.5

2.0

2.9

3.0

○
△
□ } NO HEAT TRANSFER
▽
◇

NOL HEATED BODY
TEMP.   -80° TO 360°

$\left[\dfrac{L}{h(Re)^{1/5}}\right]\dfrac{\delta}{\delta}$ NO HEAT $\begin{pmatrix}\text{PARAMETER PROPORTIONAL}\\ \text{TO THE RATIO } \delta/h\end{pmatrix}$

Figure 8

AIRFOILS
BASE PRESSURE VERSUS RATIO OF
BOUNDARY-LAYER THICKNESS TO BASE HEIGHT

Figure 9

BODIES
AFTERBODY DRAG FOR CONSTANT AFTERBODY LENGTH

Figure 10

AIRFOILS
PRESSURE DRAG FOR CONSTANT SECTION AREA

$\frac{t}{c} \approx .05$

$M_\infty = 1.5$

C_D

TOTAL

BASE

$M_\infty = 3$

TOTAL

BASE

$M_\infty = 8$

TOTAL

BASE
(VACUUM)

(TRAILING-EDGE THICKNESS)/(MAXIMUM THICKNESS), h/t

Figure 11

BODIES
EFFECT OF BASE BLEED ON BASE PRESSURE

$M_\infty = 1.9$

$\frac{p_b}{p_\infty}$

$\frac{\Delta C_{Db}}{C_{Db}} \approx 60\%$

$\beta = 9.3°$

$\frac{\Delta C_{Db}}{C_{Db}} \approx 30\%$

$\beta = 0°$

p_j/p_∞
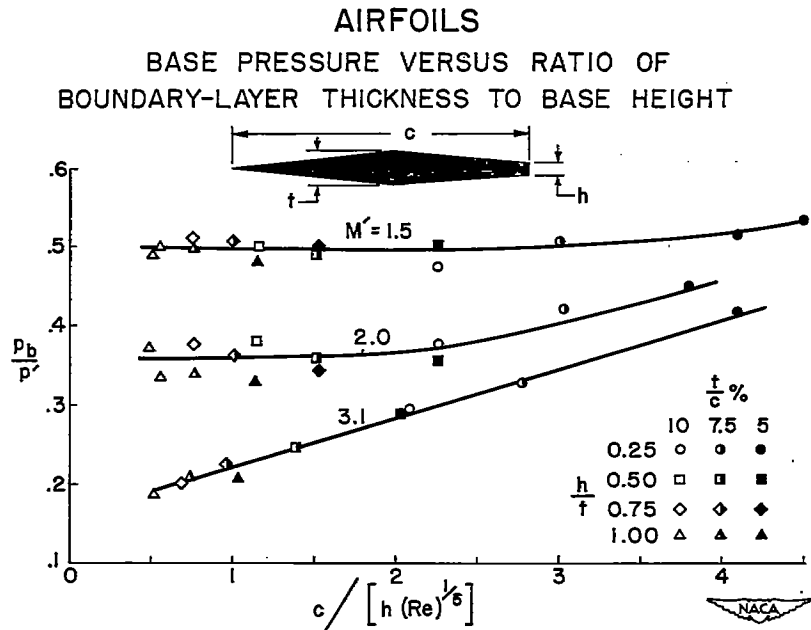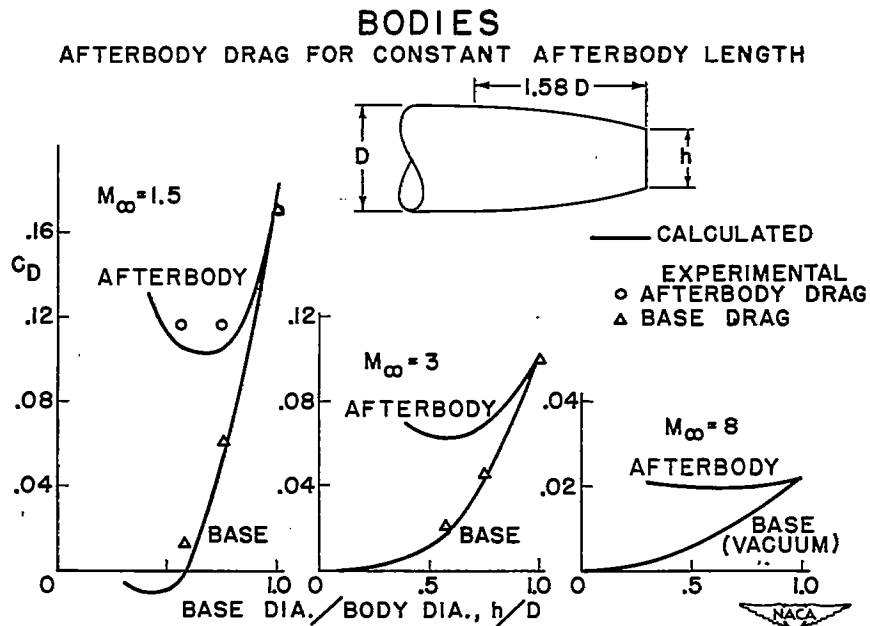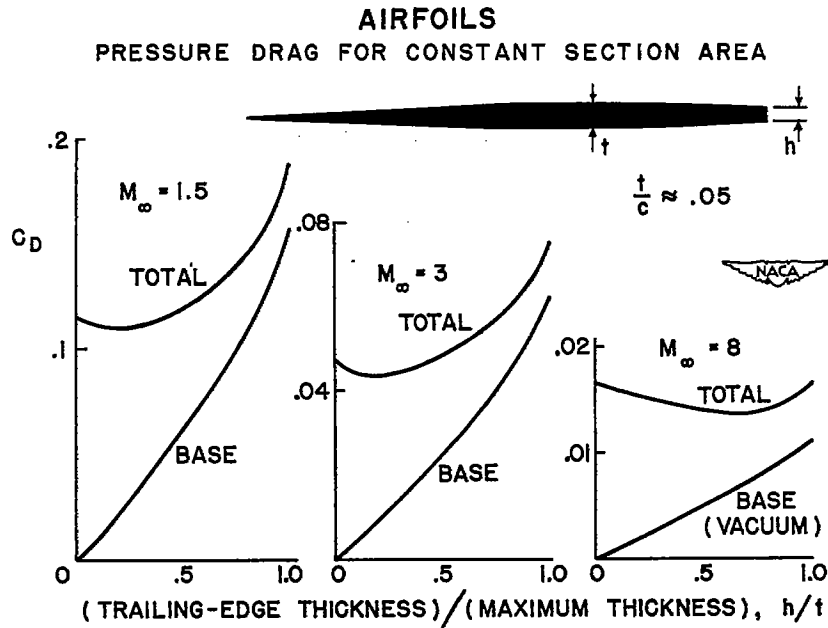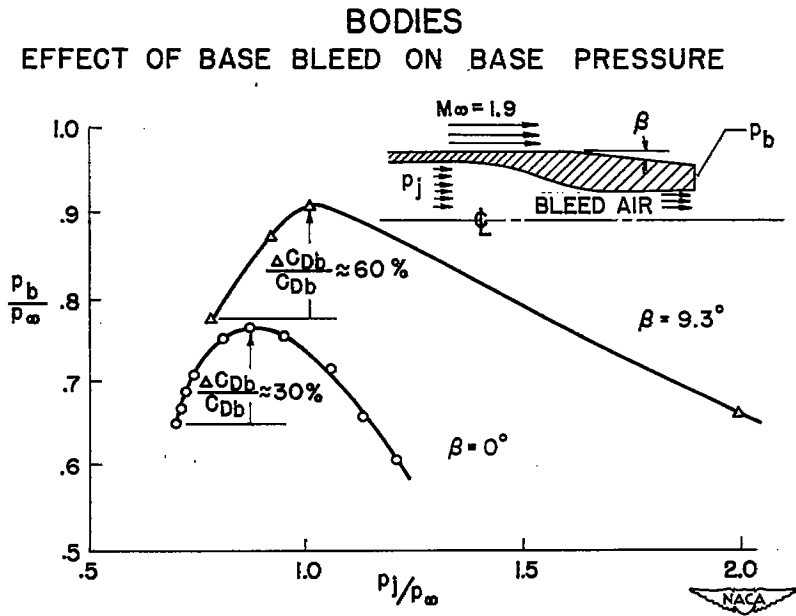
Figure 12

AIRFOILS

EFFECT OF BASE BLEED ON BASE PRESSURE

Figure 13

BODIES

EFFECT OF ANGLE OF ATTACK
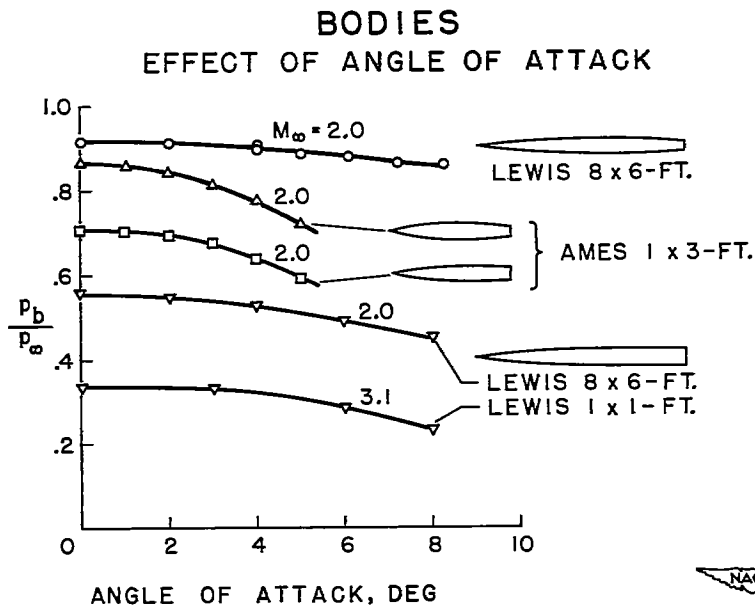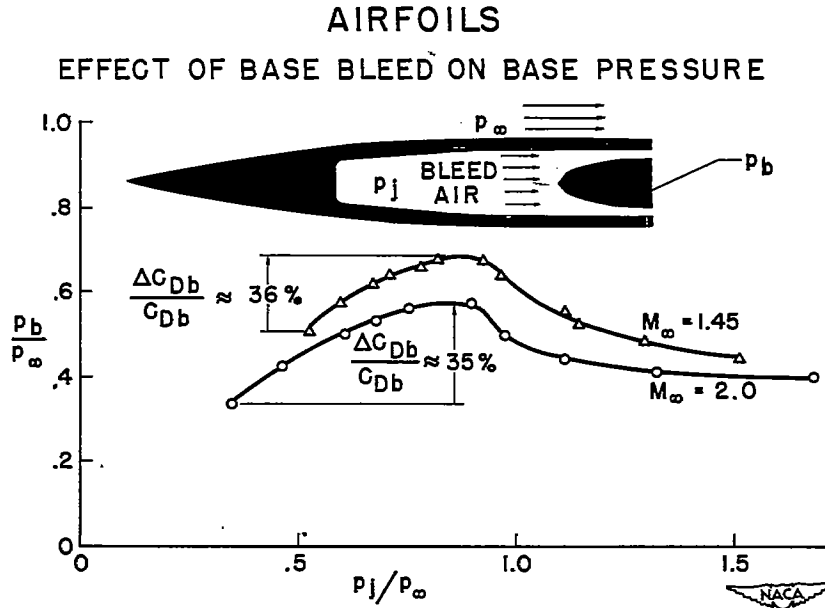
Figure 14

AIRFOILS
EFFECT OF ANGLE OF ATTACK ON BASE PRESSURE

AMES 1x3-FT

LANGLEY 9-IN.

LANGLEY 9-IN. BLOWDOWN
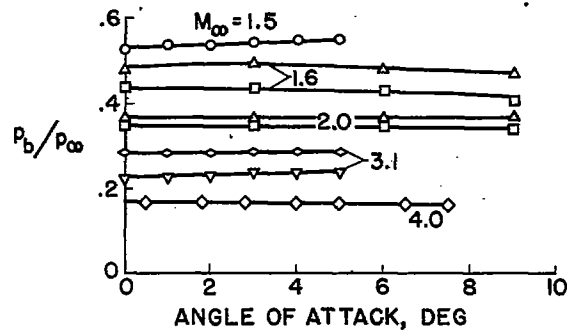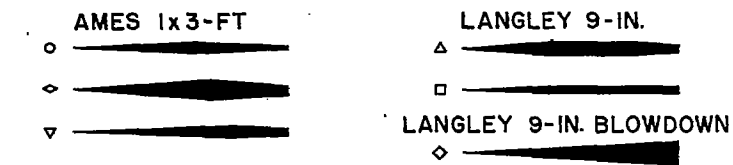
Figure 15

FLOW OVER INCLINED BODIES[1]

By E. W. Perkins and F. E. Gowen
Ames Aeronautical Laboratory

There are available at present several theoretical methods for predicting the aerodynamic characteristics of slender inclined bodies of revolution. Most of these methods are based upon potential-flow solutions and employ perturbation methods and thus suffer from two very serious limitations. First, these theories predict only initial lift-curve slopes and are therefore useful in only the very low angle-of-attack range. Second, and perhaps most important, since the theories are potential-flow solutions they fail to consider any effects of viscosity.

It has been generally observed by experimenters that the lift-curve slope of an inclined body of revolution increases with increasing angle of attack. An extension of slender-body theory by Lighthill (reference 1) includes terms in the square and cube of the angle of attack; however, the contributions of these terms at moderate Mach numbers are, in general, insufficient to account for the nonlinearity observed in the experimental data.

It has long been recognized that the effects of viscosity have an important influence on the flow over inclined bodies of revolution. Allen (reference 2) has developed a semiempirical method for calculating these effects for slender bodies as illustrated in figure 1. It has been shown that the component of velocity normal to the inclined body axis $V_0 \sin \alpha$, which results in no net force in a potential flow, contributes important forces in the cross-flow direction in a viscous fluid. These forces result from the separation of the cross flow on the lee side of the body. Thus, this so-called viscous cross force results from much the same type of flow as occurs for a circular cylinder in two-dimensional flow. Hence, in Allen's analysis the effects of viscosity on the local cross force are related to the drag of an element of a circular cylinder in two-dimensional flow. As illustrated in figure 1, one of the basic assumptions of the method is that this viscous cross force may be simply combined with a potential cross force in the calculations of the total local cross force f. In this expression q is the dynamic pressure; ds/dx is the rate of change of body-cross-section area with distance along the body; C_{d_c} is the section drag coefficient of a circular cylinder of the same local radius r at a Reynolds number and Mach number based upon the cross component of velocity; and η is a factor to allow for the decrease in section drag coefficient due to the finite length of the body. The dashed curve in figure 1 shows the potential contribution to the cross-force distribution;

[1]This is a reprint of the paper by the same authors which was presented at the NACA Conference on Aerodynamic Design Problems of Supersonic Guided Missiles at the Ames Aeronautical Laboratory on Oct. 2-3, 1951.

whereas, the solid curve includes the allowance for viscous effects. Based upon this distribution of local cross force the lift, the drag-rise, and the pitching-moment characteristics of inclined bodies may be calculated. A typical example of the comparison between experiment and theory is shown in figure 2. It is apparent that the potential theory alone is inadequate in all but the very low angle range where the viscous effects are very small.

Comparison of the result of Allen's approximate theory with the experimental force and moment characteristics for a wide variety of bodies over a large Mach number range (reference 3) showed that this simple allowance for viscous effects yields results for the lift and drag increment which are in fair agreement with experiment. However, it was noted, in general, that the center-of-pressure position was more rearward by approximately 1 body diameter than the theory predicted.

Perfect agreement with experiment would not be expected since the potential theory used applies only for very slender bodies and the viscous contribution would be expected to be exact only at stations far downstream from the nose of the body.

The results of visual flow and pressure distribution studies (reference 3) have demonstrated the similarity between the cross flow for an inclined body of revolution and the two-dimensional flow about a circular cylinder. It has been shown that the circumferential pressure distributions for the inclined body and the circular cylinder deviate from their respective theoretical inviscid distributions on the lee or downstream side in much the same manner. With the aid of a visual flow technique, it has been shown that there is a shedding of vortices within the cross-flow field of the inclined body. However, unlike the phenomenon associated with the circular cylinder, the shedding from the inclined body is not periodic. It has also been found that the vortex configuration depends to a large extent on the shape of the nose of the body.

To illustrate these effects better, vapor-screen pictures were made with the aid of the experimental setup shown in figure 3. A camera is mounted within the wind tunnel on the model support strut downstream from the model. The camera "looks" upstream and is focused on the plane of the vapor screen. The approximate field of view of the camera has been indicated. It has been generally observed that there is a stable symmetric vortex pair associated with a lifting body at low angles of attack. As the angle of attack is increased, the vortex configuration becomes asymmetric and aperiodically unsteady. Typical results obtained for a body with an ogival nose and a body with a sharp conical nose are shown in figure 4. These vapor-screen pictures show that the vortex configuration associated with the ogival-nosed body remain symmetric to a much higher angle of attack than did the configuration for the body

with the sharp conical nose. For both models in the high angle-of-attack range, the vortex configuration was asymmetric and unsteady. The unsteadiness of the flow was associated with an aperiodic switching of the vortices from side to side as illustrated in figure 5. The data in figure 5 are sequences taken from a movie which shows the change in the vortex configuration with time at two angles of attack for the model with the ogival nose. These pictures were taken at 10 frames per second and indicate the rapidity with which the vortex configuration changes in the high angle-of-attack range. The results of these vapor-screen studies show that the cross-flow wake for the ogival-nosed body is not only symmetric but is also steady to a much higher angle of attack than is the cross-flow wake for the model with the sharp conical nose.

The unsteady nature of the flow in the cross-flow wake of the inclined bodies at large angles of attack would be expected to result in erratic fluctuations in the rolling moment and side force for a missile configuration with aft surfaces which were immersed in the cross-flow wake from the lifting forebody. Since these erratic characteristics are undesirable, it is evident that of the two nose shapes for which information was presented the ogival nose had the better characteristics. The results of additional studies made with the vapor-screen technique have shown that, from the standpoint of avoiding the problems associated with the asymmetry and unsteadiness in the cross-flow wake, slender pointed nose shapes similar to the conical nose should be avoided.

Although the vapor-screen pictures serve as an indication of the presence of vortices in the cross-flow field they yield only qualitative information. To provide a quantitative measure of the flow conditions in the vicinity of the vortices, downwash measurements have been made in the plane of the base of the model. A vapor-screen photograph and the corresponding downwash distribution along a line 1.4 body radii above the body axis are shown in figure 6. At this angle of attack the vapor-screen photograph for this model with the tangent ogive nose indicates the presence of a symmetric pair of vortices on the lee side of the body and, as anticipated, the downwash measurements show a distribution characteristic of two symmetrically disposed vortices.

As was noted from figure 4, as the angle of attack was increased the vortex configuration changed from the symmetric pair to an asymmetric configuration. It has been observed that the asymmetric configuration remained steady at certain angles of attack, whereas with small changes in angle the configuration may become unsteady. Figure 7 shows a vapor-screen picture of a steady asymmetric vortex configuration and the corresponding variation of downwash along a line approximately 3 body diameters above the body center line. The stream-angle distribution is asymmetric as would be expected from the vapor-screen picture.

It appears from vapor-screen studies that the fluctuations of flow were of an aperiodic nature. However, more conclusive evidence of the aperiodicity was obtained from time histories of the static pressure fluctuations on the body. In figure 8 is shown the surface-pressure fluctuation obtained with the aid of a capacitance-type pressure cell located at the position indicated on the sketch. Although the data presented cover only a relatively short time interval, it is apparent that the pressure fluctuations are aperiodic and of varying amplitude. For the data presented, the pressure cell was at the approximate circumferential location of the vortex core. At this position and angle of attack the magnitude of the pressure fluctuations was most severe. The maximum pressure fluctuations at lower angles of attack and at other circumferential positions were of the order of one-quarter of this magnitude.

For any missile which must operate at large angles of attack and for which the tail surfaces are immersed in the vortex flow field on the lee side of the body, the asymmetric and unsteady nature of this flow will promote unexpected and erratic rolling as well as undesirable forces and moments in yaw. Although these forces in themselves may not be important, the continual fluctuation of the forces would tend to expend an intolerable amount of the available control fluid.

Wind-tunnel tests have been conducted on a number of models to determine the magnitude and frequency characteristics of the fluctuating forces. Time histories of the side force and rolling moments were obtained with the aid of a multiple-channel recording galvanometer. A series of sections from typical records are presented in figure 9. The records indicate the variation with time of the rolling and side forces at several angles of attack for the model shown schematically at the top of the figure. The records show that at 25.5° angle of attack this symmetric model was subject to a large rolling force resulting from the asymmetry of the flow in the cross-flow wake from the body. In addition to this force, which results in an average rolling-moment coefficient of approximately 0.05 based on the total area and span of the tail fin, there is a fluctuating moment resulting from the unsteadiness of the vortex flow from the forebody. With a change in angle of attack from 25.5° to 27° the average rolling moment reversed sign although the fluctuations were of about the same magnitude. With further increases in angle of attack to 28.6°, the model suffered violent fluctuations in both roll and side force. This condition corresponds to the angle of attack at which very rapid switching of the vortices from side to side was observed in the vapor-screen studies. A further increase in angle of attack resulted in another reversal in the sign of the average rolling force and a large diminution of the fluctuations.

The results of testing this model with the sharp conical nose throughout the angle-of-attack range to a maximum of approximately 34°

are shown in figure 10. On the upper graph is plotted the average
rolling moment at each angle of attack; whereas in the lower graph is
plotted the magnitude of the maximum fluctuation of the rolling moment.
It is evident from the upper graph that the average rolling moment was
small until the angle of attack exceeded approximately 23°. Above 23°
the asymmetric flow resulted in large rolling forces which varied rapidly
with angle of attack. At angles as low as 10° some fluctuations in roll
were exhibited by the model with the sharp conical nose. The maximum
value of the fluctuating rolling moment occurred at approximately
30° angle of attack. With further increase in angle of attack above 30°,
the fluctuating forces diminished. A better appreciation of the control
problem involved is obtained if one realizes that the maximum indicated
roll coefficient is that which would be developed by approximately a
12° deflection of the tail fin.

Data for a similar model with an ogival nose are shown in figure 11.
Comparison of these data with the results for the conical-nosed body show
that, although the average rolling moment due to the flow asymmetry is
of the same order of magnitude, the variation with angle of attack was
not nearly so erratic. For this model, the fluctuating component of roll
is negligibly small to an angle of attack of about 18° and the maximum
value of the fluctuating roll was only approximately half that of the
model with the conical nose. These results are in general agreement
with the indications of the vapor-screen tests where it was observed
that, for the model with the ogive nose, the flow in the cross-flow wake
was steady and the vortex configuration symmetric to higher angles of
attack than for the model with the sharp conical nose.

Shown in figure 12 are the results of some preliminary tests con-
ducted in the Ames 6- by 6-foot supersonic tunnel on a model of somewhat
higher fineness ratio. The magnitudes of the rolling-moment coefficient
are not given since some question remains as to the interpretation of
the records obtained because of the dynamic characteristics of the model
and support system. Nevertheless, the trends with increasing angle of
attack and Mach number are clearly evident. The data show the variation
of the fluctuating rolling moment with angle of attack for several Mach
numbers. The variation with angle of attack is qualitatively the same
at each of the supersonic Mach numbers and in general indicates a decrease
in magnitude with increasing Mach number. The tests at a Mach number
of 0.9 were terminated at 20° angle of attack because of the violent
oscillations of the model.

The results of recent vapor-screen studies of several bodies in
the Ames 1- by 3-foot supersonic tunnel have indicated that an increase
in Reynolds number tends to reduce the angle of attack at which unsteadi-
ness in the cross flow occurs. However, no direct correlation with
Reynolds number has been found.

It has been shown in a preceding paper by Seiff and Sandahl that the use of blunt-nosed shapes is desirable from a standpoint of drag reduction. The vapor-screen studies have shown that in addition to yielding a drag reduction the use of blunt-nosed shapes is beneficial in that an increase in the angle of attack at which unsteadiness in the cross-flow wake occurs is realized.

It is apparent that only general trends may be deduced from the results of the wind-tunnel tests since in these tests the models were rigidly mounted on a balance system which restricted their movement. It does not appear unreasonable to expect that for missiles in free flight there could be an aerodynamic coupling between the motion of the body and the shedding of the vortices such that a periodic oscillation might result. Tests which are presently being conducted by the free-fall technique should yield some information on the effects of the vortex discharge on the free-flight characteristics of a missile-like configuration.

It has been shown that the effects of viscosity on the flow over inclined bodies of revolution are important and must be considered in the calculation of the forces and moments at any appreciable angle of attack. As a result of the asymmetry and unsteadiness of the flow in the cross-flow wake from an inclined body, fluctuations in roll and side force occur for a missile-like body-tail combination at large angles of attack. The results of wind-tunnel tests have shown that the use of blunt-nosed shapes tends to alleviate the problem somewhat by increasing the useful angle-of-attack range and by reducing the magnitude of the unsteady rolling forces.

REFERENCES

1. Lighthill, M. J.: Supersonic Flow past Slender Pointed Bodies of Revolution at Yaw. Quarterly Jour. Mech. and Appl. Math., vol. 1, pt. 1, March 1948, pp. 76-89.

2. Allen, H. Julian: Estimation of the Forces and Moments Acting on Inclined Bodies of Revolution of High Fineness Ratio. NACA RM A9I26, 1949.

3. Allen, H. Julian, and Perkins, Edward W.: Characteristics of Flow over Inclined Bodies of Revolution. NACA RM A50L07, 1951.
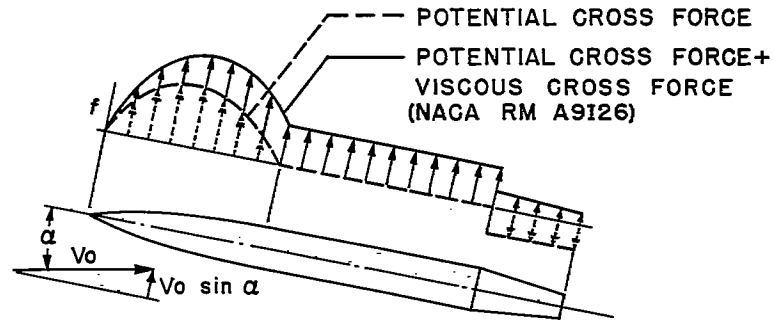
$$f = \text{POTENTIAL CROSS FORCE} + \text{VISCOUS CROSS FORCE}$$

$$= 2q \left(\frac{ds}{dx}\right)\alpha + 2\eta\, C_{d_c}\, q\, r\alpha^2$$

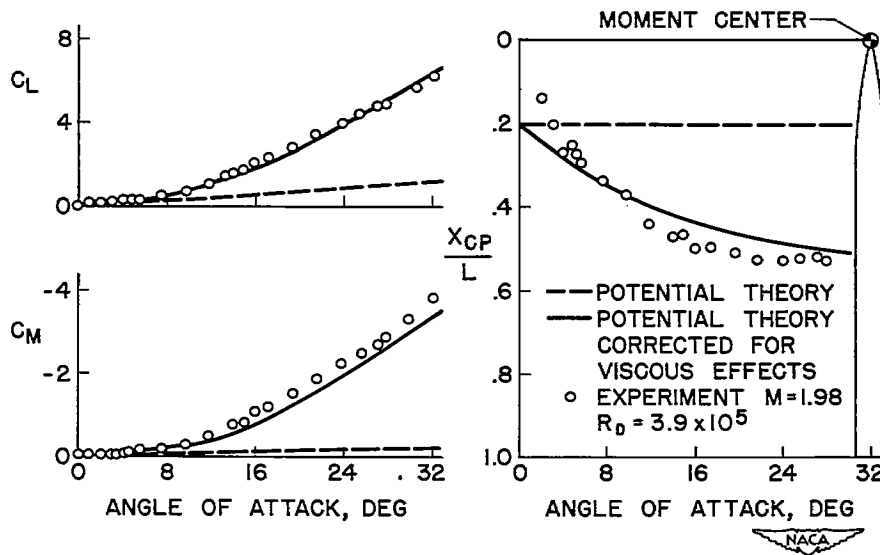Figure 1.- Schematic diagram of cross-force distribution.

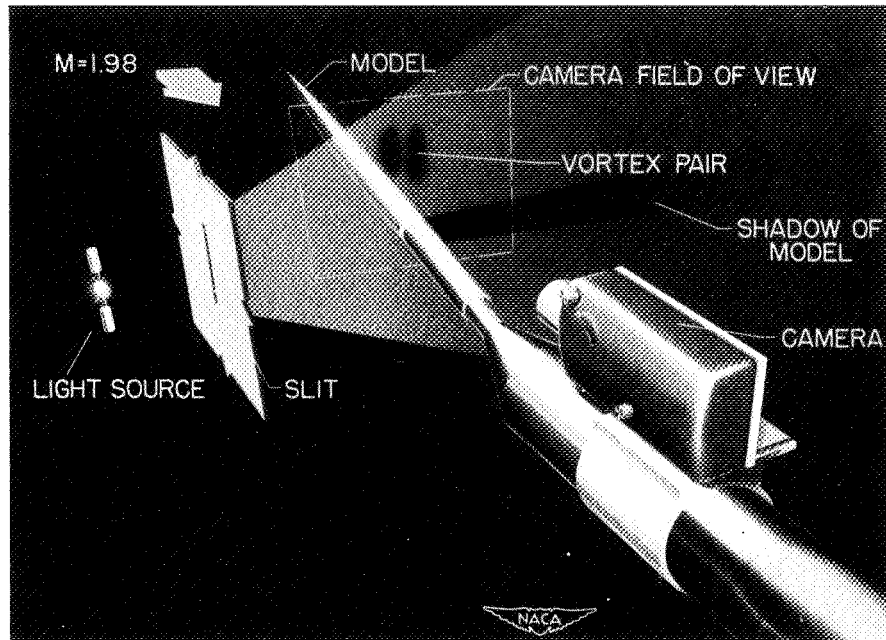Figure 2.- Typical comparison of experiment and theory.

M=1.98   MODEL   CAMERA FIELD OF VIEW

VORTEX PAIR

SHADOW OF MODEL

CAMERA

LIGHT SOURCE   SLIT

NACA

Figure 3.- Schematic diagram showing orientation of camera and model
for vapor-screen tests.
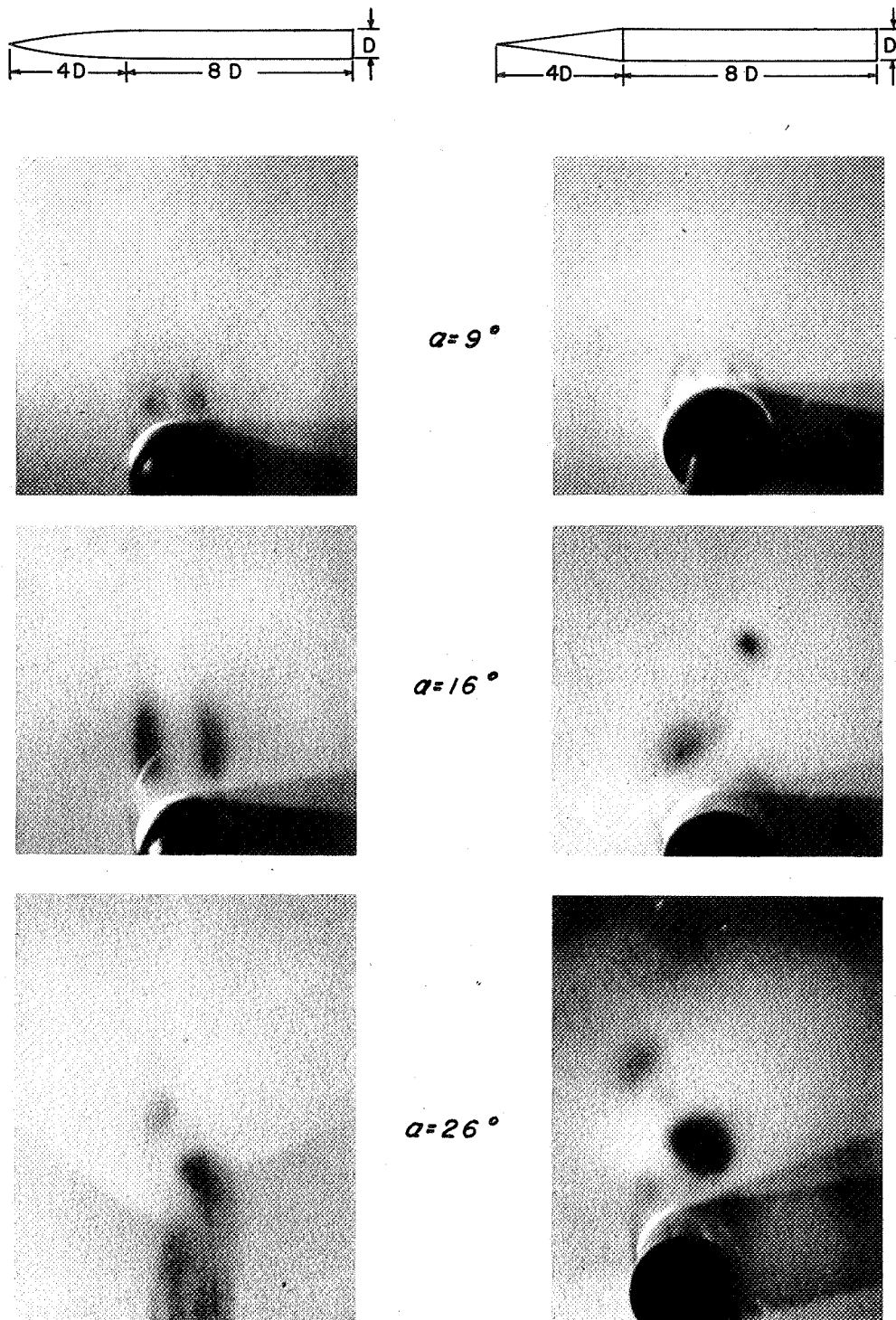
Figure 4.- Effect of nose shape on the variation with angle of attack of the vortex configuration.
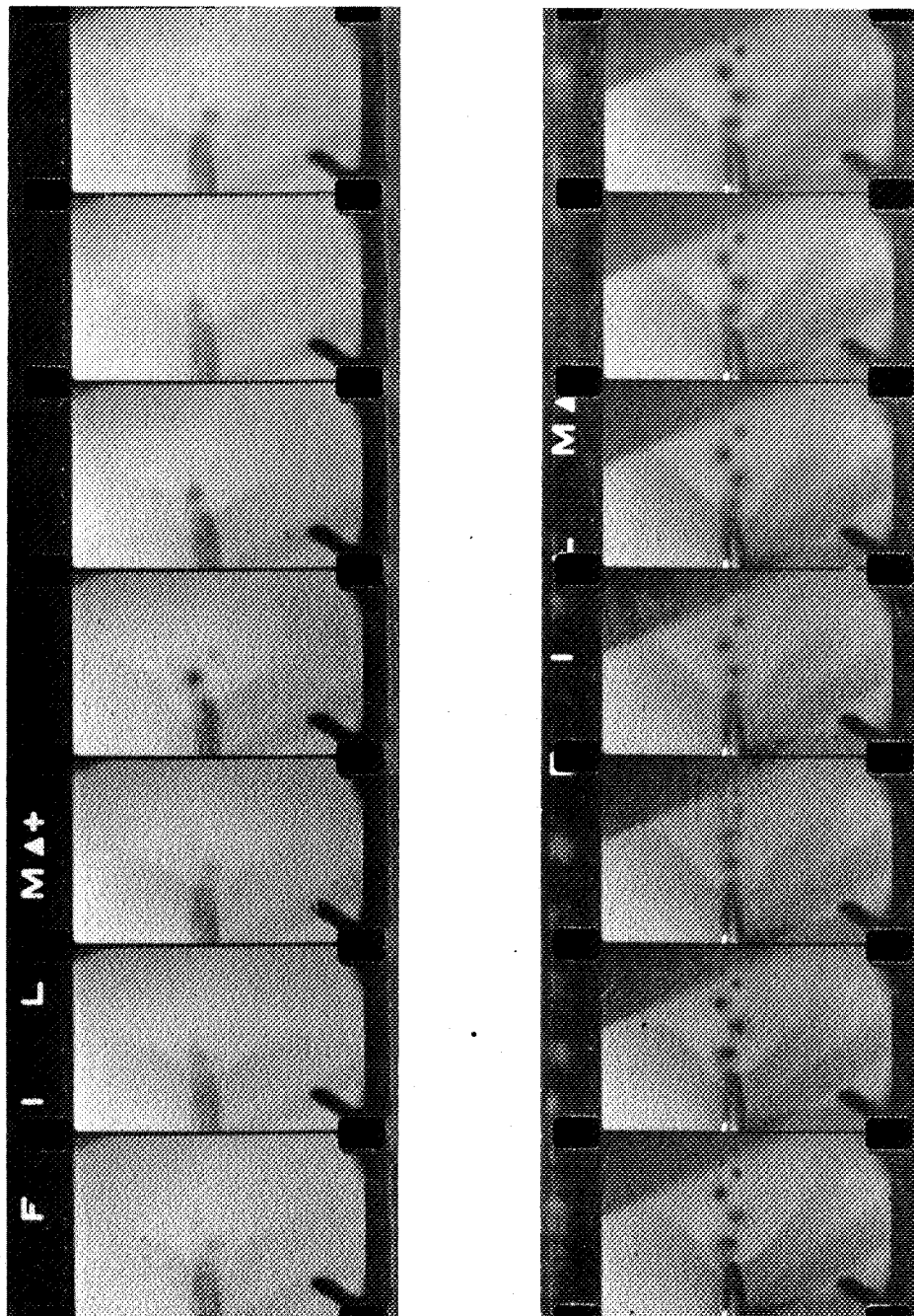
$$a = 28°$$ $$a = 36°$$

Figure 5.- Vapor-screen pictures showing fluctuation of the vortices
in the cross-flow wake of the body with the ogival nose.
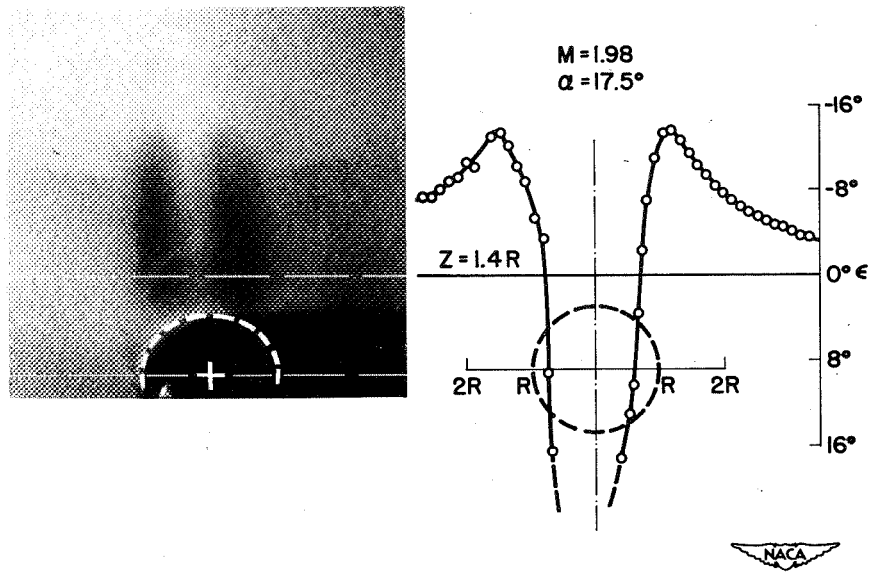
Figure 6.- Downwash distribution through vortex pair.
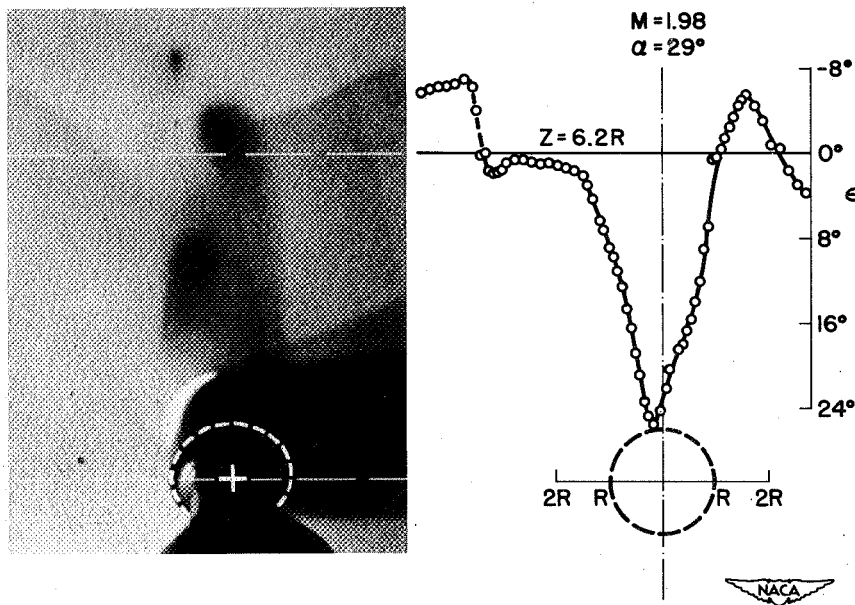
Figure 7.- Downwash distribution through asymmetric vortex configuration.
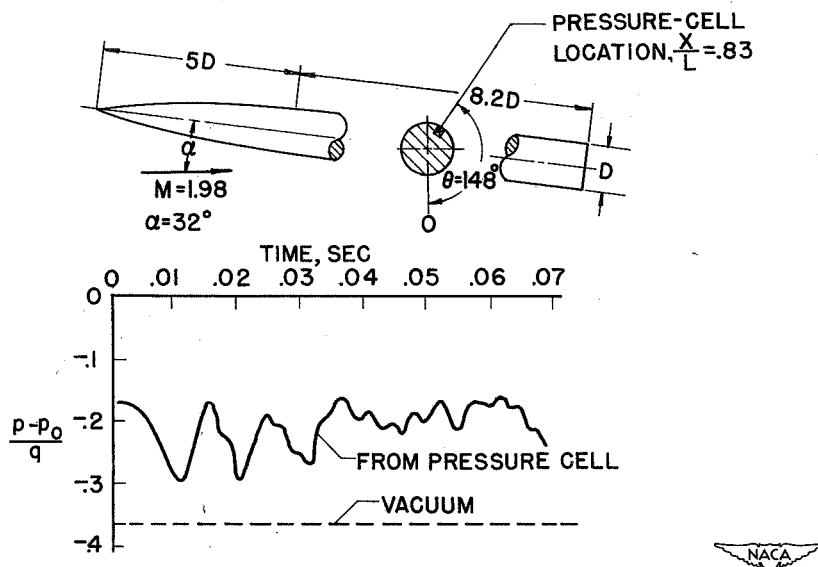
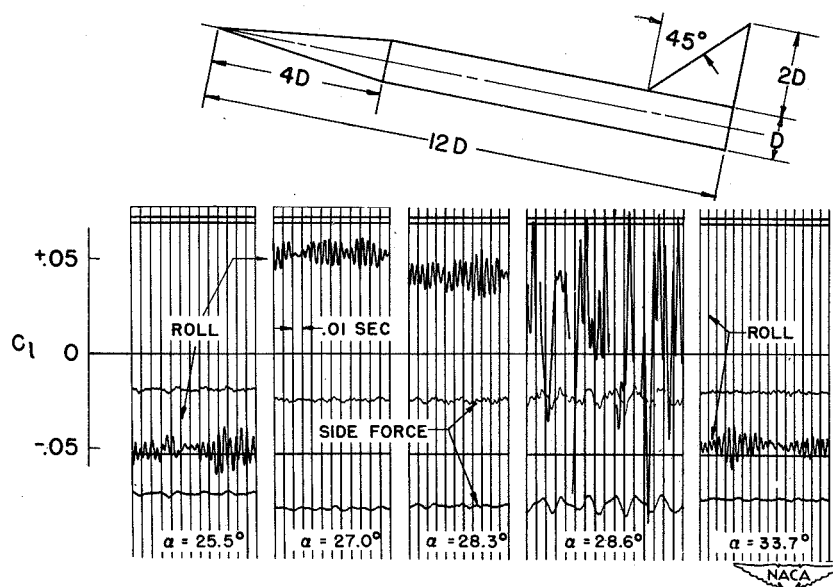Figure 8.- Surface-pressure fluctuations accompanying unsteady flow in the cross-flow wake.

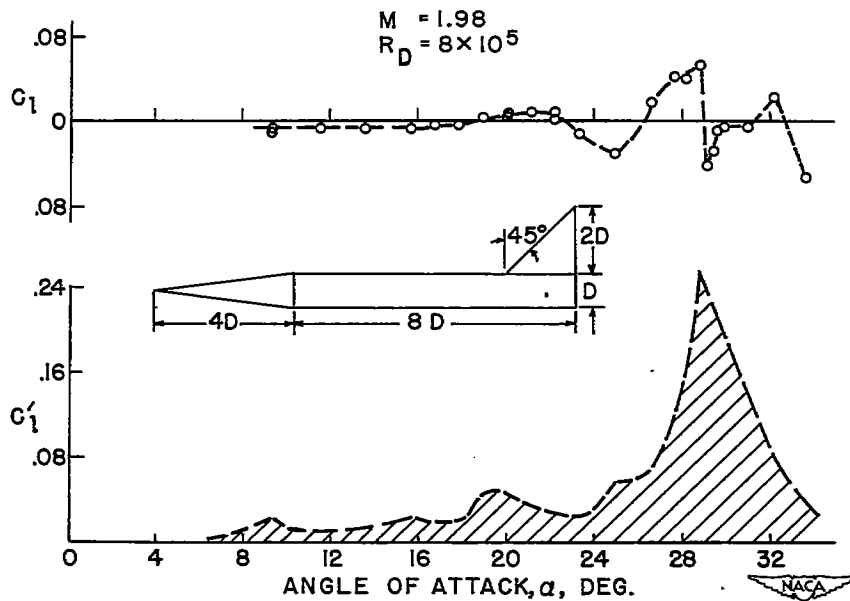Figure 9.- Typical oscillograph records of roll and side force fluctuations.

Figure 10.- Variation of the average rolling-moment coefficient and the maximum fluctuating rolling-moment coefficient for a body-tail combination with conical nose.
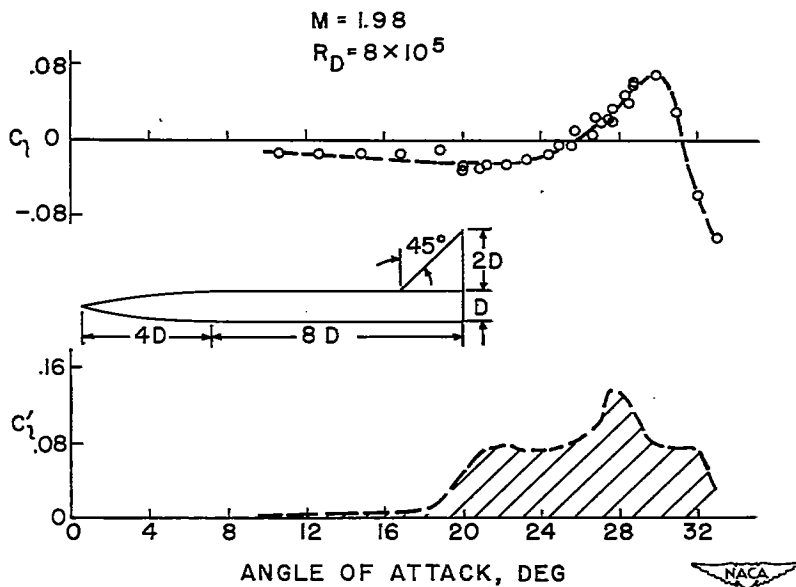

Figure 11.- Variation of the average rolling-moment coefficient and the maximum fluctuating rolling-moment coefficient for a body-tail combination with ogival nose.
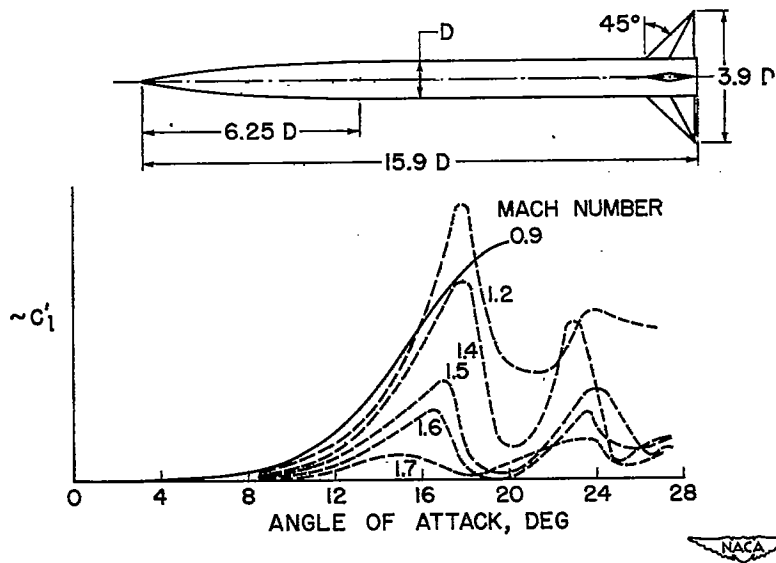
Figure 12.- Effect of Mach number on the maximum amplitude of the fluctuating rolling moment.